Numerical study of DNA-functionalized micro- and nano-particles: explicit pair potentials and their implications for phase behavior

Mirjam E. Leunissen[1, 2, a)] and Daan Frenkel[2, b)]

[1)] *FOM Institute AMOLF, Science Park 104, 1098 XG, Amsterdam, The Netherlands*

[2)] *University of Cambridge, Lensfield Road, Cambridge, CB2 1EW, UK*

(Dated: 2 February 2011)

DNA-coated colloids have great potential for the design of complex self-assembling materials. In order to predict the structures that will form, knowledge of the interactions between DNA-functionalized particles is crucial. Here, we report results from Monte Carlo simulations of the pair-interaction between particles coated with single-stranded DNA sticky ends that are connected to the surface by relatively short and stiff surface tethers. We complement our calculations with a study of the interaction between two planar surfaces coated with the same DNA. Based on our simulations we propose analytical expressions for the interaction potentials. These analytical expressions describe the DNA-mediated interactions well for particle sizes ranging from tens of nanometers to a few micrometers and for a wide range of grafting densities. We find that important contributions to both the repulsive and attractive parts of the free energy come from purely entropic effects of the discrete tethered sticky ends. Per bond, these entropic contributions have a magnitude similar to the hybridization free energy of a free pair of sticky ends in solution and they can thus considerably change the effective sticky-end binding strength. Based on the calculated interaction potentials, we expect that stable gas-liquid separation only occurs for particles with radii smaller than a few tens of nanometers, which suggests that nano-particles and micrometer-sized colloids will follow different routes to crystallization. Finally, we note that the natural statistical non-uniformities in the surface distribution of sticky ends lead to large variations in the binding strength. This phenomenon may compromise the reliability of tests that aim to detect specific DNA targets in diagnostics. In addition to guiding the design of novel self-assembling materials and gene-detection assays, the insights presented here could also shed more light on (multivalent) interactions in other systems with tethered binding groups, for instance in the areas of supramolecular chemistry or ligand-receptor mediated bio-recognition.

PACS numbers: 82.70.Dd, 82.70.Kj, 81.16.Dn, 81.16.Fg, 64.70.pv, 64.75.Yz

[a)]m.e.leunissen@amolf.nl; www.amolf.nl

[b)]df246@cam.ac.uk

I. INTRODUCTION

Over the past few years, the use of biologically-inspired specific binding groups in the fields of colloid science and nanotechnology has increased tremendously (see for example Refs.[1–4]). A particularly promising approach is to use complementary single-stranded DNA sticky ends to direct the spontaneous self-assembly of higher-order structures of small particles and other objects. Such DNA-mediated interactions offer exquisite programmability through their user-defined nucleotide sequence and are entirely reversible at moderate temperatures. However, in spite of the impressive achievements of 'pure' DNA nanotechnology (e.g. Refs.[4–7]), steering nano- and micro-colloidal assembly processes with DNA (e.g. Refs.[8–21]) still appears to be anything but straightforward. Experiments show that the behavior of DNA-coated particles in suspension strongly depends on factors such as the density of the particle's surface coverage, the binding strength of the sticky ends, the particle size and the length of the construct that tethers the sticky ends to the surface[22–30]. However, a quantitative understanding of the interactions and the resulting phase behavior[14,25,27,28,31–40] is still largely lacking. We therefore present here a numerical simulation method that allows us to generate the free energy profiles for a common class of systems, namely solid surfaces functionalized with relatively short and stiff DNA constructs, as used in for instance Refs.[10,14,23,24,27,29]. With this numerical approach, we explore the dependence of the (non-electrostatic part of the) DNA-mediated interactions on the grafting details, we derive analytical expressions for the simulated pair-interaction potential (both for planar surfaces, Eqs. 5-8, and for spherical particles with sizes in the nanometer to micrometer range, Eqs. 11-12; see also Section IV) and we predict the form of the phase diagram for DNA-functionalized particles by evaluating the strength and the range of their attractive interactions. In addition, we discuss the important but under-appreciated role that entropic effects play in the interaction between discrete tethered binding groups, as well as the implications of our results for the interpretation of some of the recent experimental observations on DNA-functionalized particles. The method and results reported in this paper should provide direct guidelines for the design of new self-assembling materials with DNA as a "smart glue". Moreover, the same fundamental insights apply to any other system with interactions mediated by tethered binding groups or multiple bonds, e.g. ligand-receptor interactions in cellular processes and drug targeting[41,42].

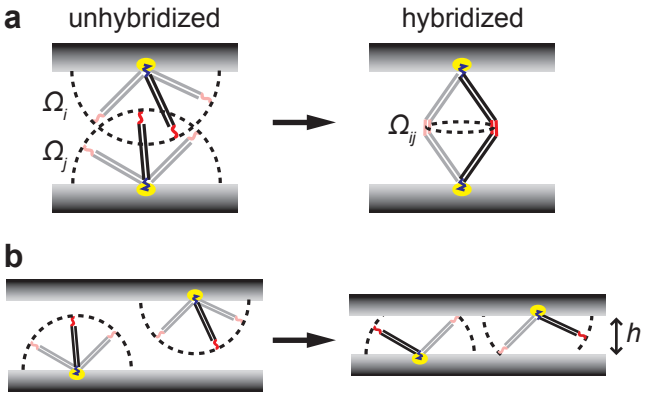

FIG. 1. Sticky end confinement. (a) Unhybridized, the tethered sticky ends (in red) explore space independently, each of them tracing the surface area of a hemi-sphere (dotted curve). Hybridized, the sticky ends explore a much smaller configurational space (Ω), because they are forced to move together. There thus is a configurational entropy cost for bond formation, as compared to free sticky ends in solution. (b) If the surface-surface separation $h < L_{\rm dna}$ the DNA constructs are confined, with their sticky endpoints tracing the surface area of a truncated hemi-sphere.

II. SIMULATION METHOD

A. Monte Carlo moves

We use Monte Carlo simulations to determine the distance-dependent interaction free energy for two surfaces functionalized with complementary DNA sticky ends. The sticky ends are tethered to the surface through a rigid 'rod-like' backbone, e.g. a short double-stranded DNA sequence (persistence length $l_{\rm p} \approx$ 45-50 nm, Ref.[43]). Each tether can swivel around its otherwise fixed attachment point to the surface, so that in the unhybridized state the sticky endpoint traces the surface area of a hemi-sphere. When two sticky ends i and j hybridize they are forced to move together (Fig. 1a) and in Refs.[27–29] and Appendix A 1 we show how this restricted freedom of motion leads to a configurational entropy cost, $\Delta S_{\rm conf}$, that needs to be added to the hybridization free energy of the sticky sequences when they are free in solution:

$$\Delta G_{\rm ij,tether} = \Delta G^0_{\rm ij,solution} - T\Delta S_{\rm conf} = \Delta G^0_{\rm ij,solution} - k_{\rm B}T \ln\left(\frac{\Omega_{\rm ij}}{\Omega_{\rm i}\Omega_{\rm j}}\frac{1}{\rho^0}\right) \qquad (1)$$

Here, $k_{\rm B}$ is the Boltzmann constant, T is the absolute temperature, ρ^0 is the standard number density (corresponding to 1 mol/liter) and $\Omega_{\rm i,j,ij}$ is the 'configurational space' of, respectively,

the freely swiveling i and j sticky ends and the bound $i-j$ pair. The configurational freedom depends on the interaction geometry, e.g. the surface-surface separation, h, and the relative positions of the surface attachment points of the DNA constructs; explicit expressions are derived in Appendix A 2-A 3 for plate-plate and sphere-sphere geometries. Although we use L_{dna}, the length of the DNA construct, as the unit of length in all of our calculations we will sometimes explicitly include L_{dna} in our derivations for the sake of clarity.

In our simulations, the DNA attachment points are Poisson distributed over the two surfaces, such that their average spacing, hereafter referred to as the 'average strand spacing' S_{dna}, satisfies a predefined value; the average surface coverage then is $1/S_{\mathrm{dna}}^2$ strands per unit area. The diameter of the DNA double helix, $d_{\mathrm{dna}} \approx 2$ nm, sets the minimum strand spacing. We average the simulation results over multiple, independently generated DNA distributions. For each distribution we determine the total interaction free energy for a series of surface-surface separations $h \in [0, 2]\ L_{\mathrm{dna}}$, at a particular value of $\Delta G^0_{\mathrm{ij,solution}}$ (hereafter abbreviated to ΔG^0), which corresponds to a temperature that is unique to the sticky DNA sequence under consideration via $\Delta G^0_{\mathrm{dna}} = \Delta H^0_{\mathrm{dna}} - T\Delta S^0_{\mathrm{dna}}$. Here, $\Delta H^0_{\mathrm{dna}}$ and $\Delta S^0_{\mathrm{dna}}$ are the standard hybridization enthalpy and entropy, respectively, of the DNA sequence when it is free in solution.

In each trial move, we randomly select a DNA strand, i, on one of the surfaces, which may be unbound or bound to a strand, j_1, on the opposing surface. We identify all the strands $j_2, j_3, ...j_{\mathrm{N}}$ on the opposing surface that are not bound to other sticky ends and that are within reach of i and we calculate the configurational entropy cost and, using Eq. 1, the Boltzmann weight $w_{\mathrm{ij_n}} = \exp\left[-\beta\Delta G_{\mathrm{ij_n}}\right]$ of each binding configuration $i-j_{\mathrm{n}}$, including $i-j_1$ ($\beta = 1/k_{\mathrm{B}}T$). The probability to form a particular bond ij_{n} then is:

$$P_{\mathrm{ij_n}} = \frac{w_{\mathrm{ij_n}}}{1 + \sum_{j_{\mathrm{N}}} w_{\mathrm{ij_n}}}$$

whereas the probability to form no bond at all is:

$$P_{\mathrm{unbound,i}} = \frac{1}{1 + \sum_{j_{\mathrm{N}}} w_{\mathrm{ij_n}}}$$

where the free energy of the unbound configuration is zero. After each move we update the identity of the binding partners and the total number of bonds.

B. Free energy calculation

The DNA-mediated interaction free energy can be obtained by thermodynamic integration (using a 10 point Gauss-Legendre quadrature) with $\langle n_{\mathrm{bonds}} \rangle_{\Delta \mathrm{G}^0}$, the average number of bonds that is formed at a specific ΔG^0, as the order parameter (see Appendix B for more details):

$$\frac{F_{\mathrm{dna-bound}}}{k_{\mathrm{B}}T}(h) = \frac{F_{\mathrm{dna-unbound}}}{k_{\mathrm{B}}T}(h) - \int_{\Delta G^{0\prime}}^{0} \langle n_{\mathrm{bonds}} \rangle_{\Delta \mathrm{G}^0,\,\mathrm{h}}\, d\Delta G^0 \tag{2}$$

Here, $F_{\mathrm{dna-unbound}}(h)$ is the interaction free energy of the DNA-functionalized surfaces at separation h if no hybridization of the sticky ends takes place and thus is simply the repulsive free energy contribution due to confinement of the DNA constructs between the two surfaces when $h < L_{\mathrm{dna}}$ (Fig. 1b):

$$\frac{F_{\mathrm{dna-rep}}}{k_{\mathrm{B}}T}(h) = -\sum_{N_{\mathrm{total}}} \ln\left(\frac{\Omega_{\mathrm{n,confined}}}{\Omega_{\mathrm{n,unconfined}}}\right) \tag{3}$$

Here, we take the case of fully non-interacting surfaces ($h > 2\ L_{\mathrm{dna}}$) as the unconfined reference state and we sum over the total number of DNA strands in the system. The expressions for $\Omega_{\mathrm{un/confined}}$ for a particular strand n can be found in Appendix A 2-A 3. In our description, we ignore direct strand-strand interactions, be they of steric or electrostatic origin. For typical DNA constructs and surface coverages we expect the contribution to $F_{\mathrm{dna-rep}}$ due to the self-avoiding character of 'real' DNA to be fairly small, as for two overlapping rigid rods the fraction of configurational space that is excluded is approximately $L_{\mathrm{dna}}^2 d_{\mathrm{dna}} / L_{\mathrm{dna}}^3 \approx 2/20 = 0.1$. We further note that, for the typical ionic strengths used in the experiments, the electrostatic repulsion between the negatively charged DNA constructs is strongly screened and its main effect is to increase the effective 'hard-core' diameter of the DNA rods. Of course, at high grafting densities, strand-strand interactions are important and the present approach would need to be refined. Realizing that the integral on the right hand side of Eq. 2 represents the attractive free energy contribution due to hybridization of the sticky ends, we use the following notation in the remainder of this article to distinguish the different contributions to the total DNA-mediated interaction free energy:

$$F_{\mathrm{dna-total}}(h) = F_{\mathrm{dna-rep}}(h) + F_{\mathrm{dna-att}}(h) \tag{4}$$

III. RESULTS AND DISCUSSION

A. Planar surfaces

To determine the interactions of two DNA-functionalized flat surfaces we averaged the results over three simulation runs with independent strand distributions, using $N_{\rm plate} = 2500$ strands/plate, the appropriate surface area, $A_{\rm plate}$, in order to obtain the desired average strand spacing ($S_{\rm dna}$), and $L_{\rm dna} = 20$ nm because many experiments are done in the 15-25 nm range. In each run, we first equilibrated the system for 50 cycles and then calculated average properties over 150 cycles, with 12500 trial moves per cycle.

1. Interaction potential

The total, surface separation dependent, plate-plate interaction free energy, $F_{\rm plate,total}(h)$, is made up of several contributions. First of all, for $h > 2\ L_{\rm dna}$, the interaction free energy vanishes (neglecting possible electrostatic interactions, as these usually are strongly screened). Then, at shorter distances, we have:

$$\begin{cases} F_{\rm plate,dna-att}(h), & 0 \leqslant h \leqslant 2\ L_{\rm dna} \\ F_{\rm plate,dna-rep}(h), & 0 \leqslant h < L_{\rm dna}\ , \end{cases}$$

and finally for $h < 0$, $F_{\rm plate,HC} = \infty$ – this is the hard-core repulsion due to overlap of the plates. Note that we do not show the hard core repulsion explicitly in any of our figures, we only plot the DNA-mediated contributions. The repulsive ($F_{\rm plate,dna-rep}$) and attractive ($F_{\rm plate,dna-att}$) contributions to the DNA-mediated interaction, as defined in Section II B, can be obtained separately from our simulations (Fig. 2a) and in the following we will first derive some useful expressions for these free energies, before discussing the general properties of the overall plate-plate interaction.

The (non-electrostatic part of the) DNA-mediated repulsion is due to confinement of the sticky ends between the two surfaces and, using Eq. 3 and $N_{\rm plate}/A_{\rm plate} = 1/S_{\rm dna}^2$, we can derive an exact analytical expression for this contribution per unit area:

$$\frac{F_{\rm plate,dna-rep}}{k_{\rm B}T\ L_{\rm dna}^2}(h) = -\frac{2}{S_{\rm dna}^2} \ln h \tag{5}$$

Here, $S_{\rm dna}$ and h are expressed in units of $L_{\rm dna}$.

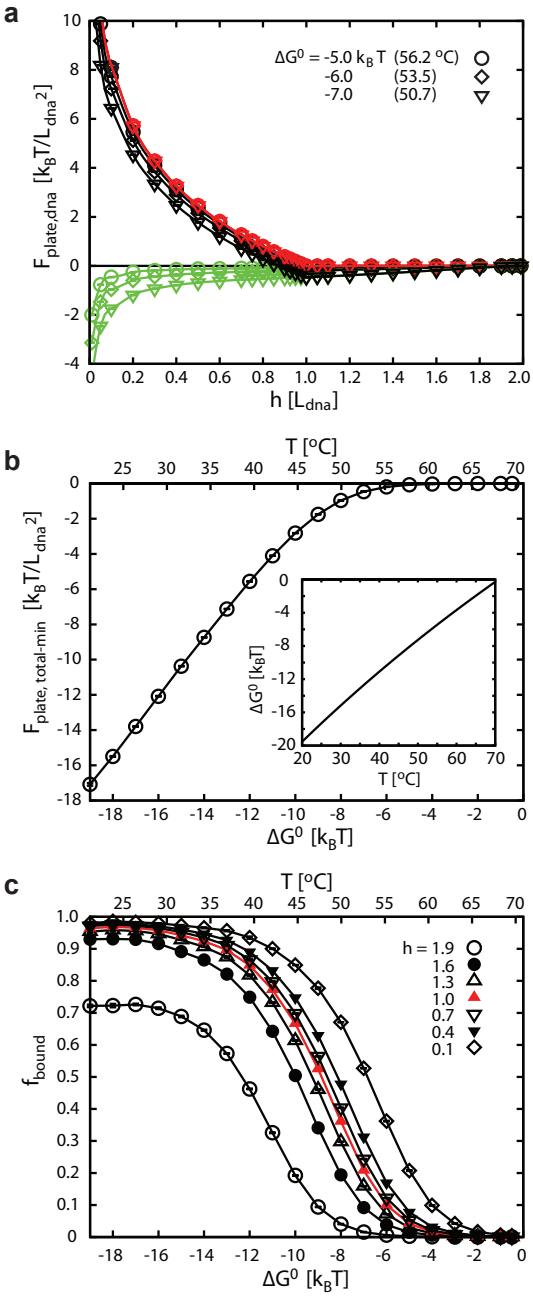

FIG. 2. Simulated plate-plate interaction for $S_{\rm dna} = 0.75\ L_{\rm dna}$. (a) Plot of the total DNA-mediated interaction free energy per unit area ($F_{\rm plate,dna-total}$, black) and the separate repulsive ($F_{\rm plate,dna-rep}$, red) and attractive ($F_{\rm plate,dna-att}$, green) contributions, as a function of the surface separation h and for different sticky-end binding strengths ΔG^0. (b) The minimum plate-plate interaction free energy at $h = 1.0$ (main panel) and the hybridization free energy of sticky ends in solution as a function of the temperature (inset; $\Delta H^0_{\rm dna} =$ -322 kJ/mol and $\Delta S^0_{\rm dna} =$ -936 J/molK). (c) The fraction of sticky ends that is bound, for different plate separations.

TABLE I. The fit constants in $F_{\text{plate,dna-att}}$ (Eqs. 7-8)

	$0 \leqslant h < 1$	$1 \leqslant h \leqslant 2$
c_1	1.24×10^{-4}	1.34×10^{-5}
c_2	-1.05×10^{-8}	6.27×10^{-6}
c_3	3.49×10^{-13}	-7.03×10^{-6}
c_4	-3.68×10^{-18}	5.90×10^{-6}

Unfortunately, we do not have an exact analytical form for the attractive contribution, because of the vast number of different ways in which the sticky ends can hybridize between the two surfaces. Instead, we determine the h dependent polynomial that captures the difference between our simulation data and the approximate expression $F_{\text{plate,dna-att,approx}}$, a derivation of which can be found in Appendix C. From the form of $F_{\text{plate,dna-att,approx}}$, the polynomial corrections are expected to depend on the surface coverage and binding strength as $S_{\text{dna}}^{-m} \exp\left[-\beta \Delta G^0\right]^n$. Using the Levenberg-Marquardt method[44], we fit trial polynomials to the data by a simultaneous unweighted least-squares minimization over all $F_{\text{plate,dna-att}}$ curves that correspond to a minimum in the total free energy $F_{\text{plate,total-min}} \in [-2.00, -0.01]$ $k_{\text{B}}T/L_{\text{dna}}^2$ and with $S_{\text{dna}} \in [0.25, 5.00]$ L_{dna} and $\Delta G^0 \in [-12.0, -1.0]$ $k_{\text{B}}T$. We find that for a satisfactory result – a combination of exponents that fits the data well while keeping the total number of terms in the polynomial as small as possible – we have to fit the data for $0 \leqslant h < L_{\text{dna}}$ and for $L_{\text{dna}} \leqslant h \leqslant 2$ L_{dna} separately, while excluding the sharp downturn in $F_{\text{plate,dna-att}}$ for $h \lesssim 0.2$ L_{dna} (Fig. 2a). This has no big impact on the overall fit to $F_{\text{plate,dna-total}}$ though, because at these small surface separations the DNA-mediated repulsion, as given by Eq. 5, generally dominates the interaction. Fitting 1534 data points in total, we find the following combination of expressions for the DNA-mediated attraction, with a residual error of ± 0.004 $k_{\text{B}}T/L_{\text{dna}}^2$ per point (the standard deviation of the simulation data typically lies around 0.001 $k_{\text{B}}T/L_{\text{dna}}^2$):

$$\frac{F_{\text{plate,dna-att,approx}}}{k_{\text{B}}T\ L_{\text{dna}}^2}(h) = -\frac{1}{S_{\text{dna}}^2} \ln\left(1 + \exp\left[-\beta \Delta G^0\right] \frac{1}{2\pi \rho^0 S_{\text{dna}}^2 A}\left[\frac{\pi}{3}(4-h^2)^{\frac{3}{2}} - B\right]\right) \quad (6)$$

with S_{dna} and h in units of L_{dna}, the standard number density $\rho^0 = 4817.7\ L_{\text{dna}}^{-3}$ for $L_{\text{dna}} =$

20 nm, and A / B as specified below:

$$A = \begin{cases} 1, & 1 \leqslant h \leqslant 2 \\ h^2, & 0 \leqslant h < 1 \end{cases}$$

$$B = \begin{cases} 0, & 1 \leqslant h \leqslant 2 \\ \int_{r_{\perp,1}}^{r_{\perp,2}} 4r_\perp \sqrt{1-\frac{1}{4}(h^2+r_\perp^2)}\, \arccos\left[\frac{h\sqrt{h^2+r_\perp^2}}{2r_\perp\sqrt{1-\frac{1}{4}(h^2+r_\perp^2)}}\right] dr_\perp, & 0 \leqslant h < 1 \end{cases}$$

Here, $r_{\perp,1,2} = \sqrt{2-h^2 \mp 2\sqrt{1-h^2}}$, where $r_\perp$ is the length of the surface projection of the vector $\mathbf{r}_{\mathrm{ij}}$ that connects the attachment points of two binding partners i and j (see also Appendix C). For $0 \leqslant h < 1$:

$$\begin{aligned} &\frac{F_{\mathrm{plate,dna-att}}}{k_\mathrm{B}T\, L_\mathrm{dna}^2}(h) = \frac{F_{\mathrm{plate,dna-att,approx}}}{k_\mathrm{B}T\, L_\mathrm{dna}^2}(h) \\ &+ \left(c_1 S_\mathrm{dna}^{-4} \exp\left[-\beta\Delta G^0\right] + c_2 S_\mathrm{dna}^{-6} \exp\left[-2\beta\Delta G^0\right]\right. \\ &\left. + c_3 S_\mathrm{dna}^{-8} \exp\left[-3\beta\Delta G^0\right] + c_4 S_\mathrm{dna}^{-10} \exp\left[-4\beta\Delta G^0\right]\right)(1-h)^2 \end{aligned} \tag{7}$$

For $1 \leqslant h \leqslant 2$:

$$\begin{aligned} &\frac{F_{\mathrm{plate,dna-att}}}{k_\mathrm{B}T\, L_\mathrm{dna}^2}(h) = \frac{F_{\mathrm{plate,dna-att,approx}}}{k_\mathrm{B}T\, L_\mathrm{dna}^2}(h) \\ &+ \left(c_1 S_\mathrm{dna}^{-3} + c_2 S_\mathrm{dna}^{-5}\right) \exp\left[-\beta\Delta G^0\right](2-h) \\ &+ \left(c_3 S_\mathrm{dna}^{-3} + c_4 S_\mathrm{dna}^{-5}\right) \exp\left[-\beta\Delta G^0\right](2-h)^2 \end{aligned} \tag{8}$$

The fit constants c_{1-4} are listed in Table I. We point out that one could derive other functional forms for the interactions as well. However, polynomials are very user-friendly and we find that they describe the data much better than any other functional form that we have tried.

The example curves in Fig. 2a show the different DNA-mediated contributions to $F_{\mathrm{plate,total}}$ for one particular surface coverage and three different ΔG^0 values, which are also relevant to experiments with spherical colloidal particles (further treated in Section III C). For illustrative purposes, we indicate some typical temperatures corresponding to these ΔG^0 values, where we use throughout this article ΔH^0_dna = -322 kJ/mol and ΔS^0_dna = -936 J/molK from Ref.[27]. The downturn in $F_{\mathrm{plate,dna-att}}$ for small plate separations is due to

an increasing confinement of the DNA constructs, which makes it relatively less costly to bind their sticky ends together (i.e. in Eq. 1 the ratio between Ω_{ij} and $\Omega_{\mathrm{i,j}}$ becomes more favorable), and this strongly enhances the overall binding. If we take the DNA-mediated repulsion into account, however, the minimum in the total free energy, $F_{\mathrm{plate,total-min}}$, always occurs at $h = 1.0$, because for smaller plate separations the number of sticky ends that interact with each other does not change much, while the repulsion increases strongly. In Fig. 2b we plot $F_{\mathrm{plate,total-min}}$ as a function of $\Delta G^0(T)$, where the latter quantity basically reflects the binding strength of a 'free' pair of sticky ends in solution at a certain temperature. Contrary to ΔG^0 (see inset), the minimum plate-plate binding free energy is not a linear function of the temperature, although it crosses over to a nearly linear regime at low temperatures, in this case when $\Delta G^0 \lesssim -12\ k_{\mathrm{B}}T$. Fig. 2c provides an explanation for this behavior: when the temperature is reduced the number of bonds initially increases strongly, but by the time ΔG^0 reaches -12 $k_{\mathrm{B}}T$ the fraction of sticky ends that is bound is already 85 % at the equilibrium separation $h = 1.0$ and the curve starts to level off. A further reduction of the temperature then leads mostly to stronger individual bonds, instead of significantly more bonds.

2. Entropic effects

Interestingly, in addition to the DNA-mediated entropic repulsion, entropic effects make an important contribution to the attractive interaction of DNA-functionalized surfaces. In Fig. 1a and Eq. 1 we already introduced the so-called configurational entropy cost which is associated with the hybridization of tethered DNA and which results from the restricted freedom of motion of the sticky ends upon binding. The other entropic effect is a 'combinatorial' entropy gain, which originates from the many different ways in which a certain number of bonds can form between the two surfaces, as there are numerous sticky ends that each have multiple possible binding partners within reach (in the simple quantitative models of Refs.[27–29] this effect was treated in an approximate fashion). The combinatorial contribution is reminiscent of the 'entropic cooperativity'[33] and 'bond disorder'[36,40] effects that have been identified before in simulation studies of DNA-functionalized particle systems with, respectively, DNA linkers freely suspended in solution and long DNA with a radius of gyration comparable to the size of the particles. A similar effect was also observed in the mean-field

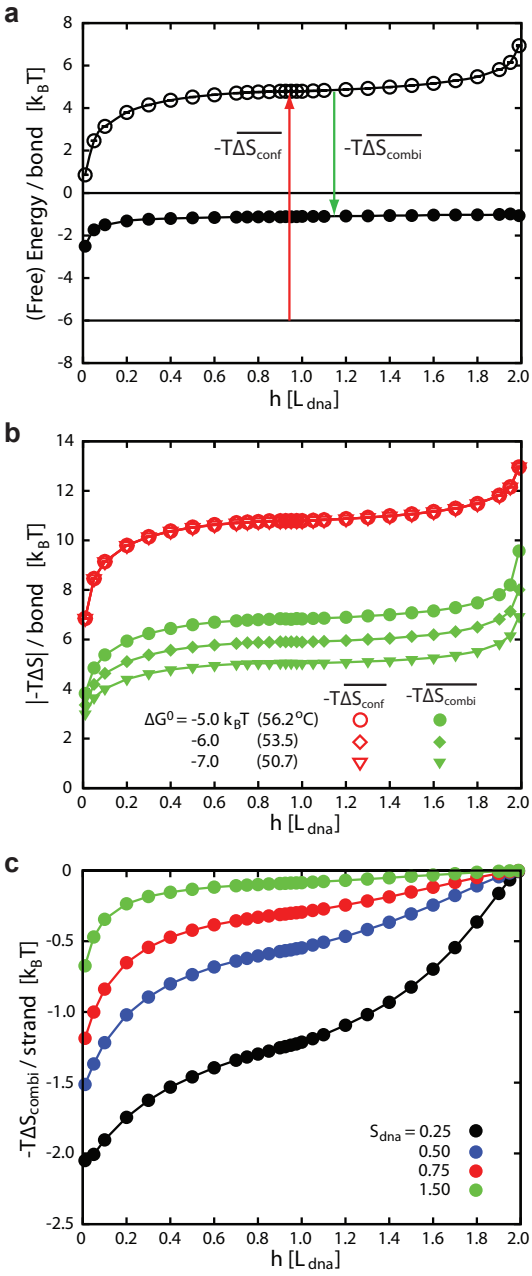

FIG. 3. Entropic contributions to the attractive plate-plate interaction. (a) Plot of the hybridization free energy of sticky ends in solution (ΔG^0, solid line) and the surface separation dependent average binding free energy per bond ($F_{\rm bond}$, solid symbols) and average bond energy ($U_{\rm bond}$, open symbols), as defined in the text. The arrows indicate the differences between the curves that correspond to the average configurational entropy cost ($-T\overline{\Delta S_{\rm conf}}$) and the average combinatorial entropy gain ($-T\overline{\Delta S_{\rm combi}}$), both per bond. The simulations were done for $S_{\rm dna} = 0.75\ L_{\rm dna}$ and $\Delta G^0 = -6.0\ k_{\rm B}T$. (b) The absolute values of $-T\overline{\Delta S_{\rm conf}}$ (red) and $-T\overline{\Delta S_{\rm combi}}$ (green), for $S_{\rm dna} = 0.75\ L_{\rm dna}$ and different ΔG^0. (c) The combinatorial entropy gain per strand for $\Delta G^0 = -6.0\ k_{\rm B}T$ and different $S_{\rm dna}$. The surface area in the simulations was chosen such that in all cases there were 2500 strands per plate.

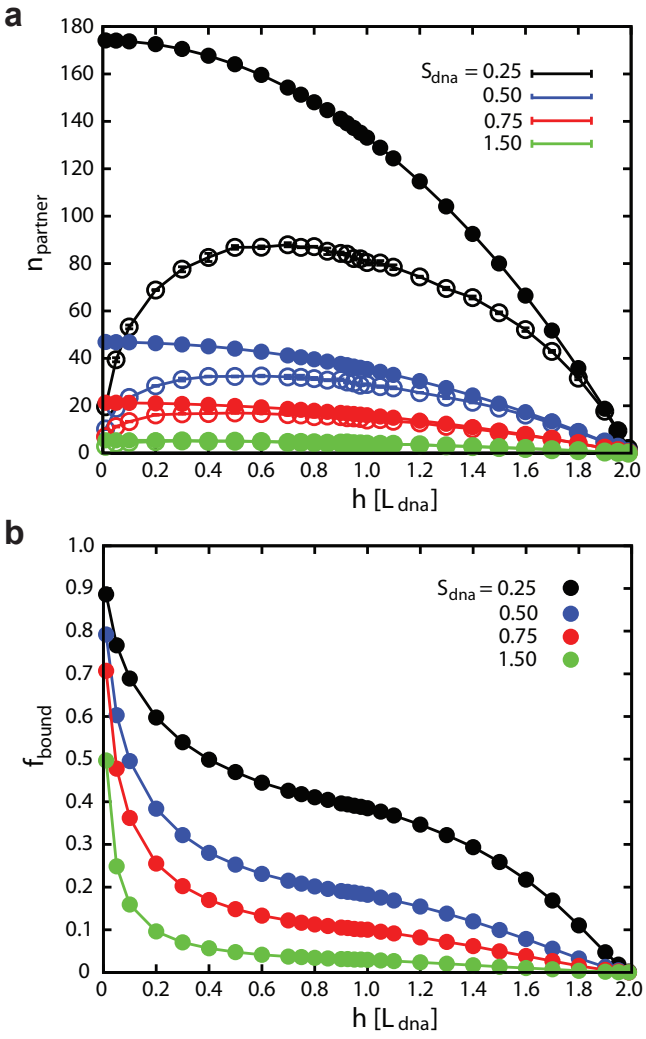

FIG. 4. Bond statistics for flat plates, averaged over simulations at $\Delta G^0 = -6.0\ k_B T$ and different S_{dna}. (a) The average number of sticky ends on the opposing surface that is within geometrical reach of a particular sticky end on the other surface (solid symbols), and the number of these that is 'free', i.e. not bound to any other sticky ends (open symbols). (b) The fraction of all sticky ends in the system that is bound, as a function of the surface separation.

theory of Zilman *et al.* for telechelic polymers[45]. These entropic effects have a major impact on the DNA-mediated interactions and phase behavior with, as the most extreme case, a first-order gas-liquid separation solely driven by the higher degeneracy of bond formation in the dense phase[36,40]. Together with the observations presented here, these results show that for a proper interpretation of suspension behavior due to tethered DNA sticky ends or other binding groups it is absolutely necessary to take the entropic effects of the bonds

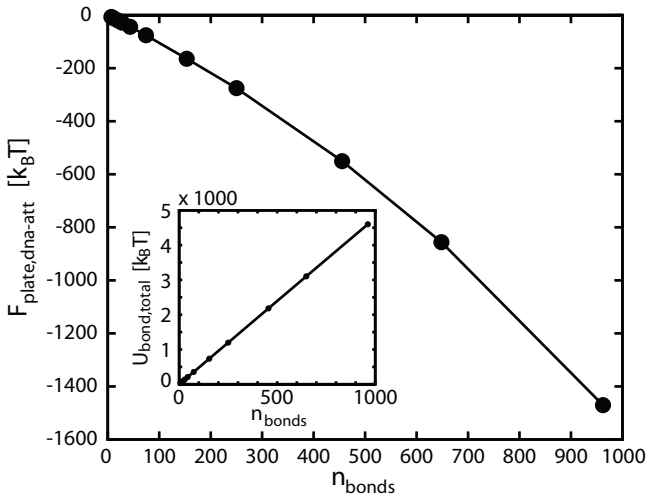

FIG. 5. The attractive contribution to the DNA-mediated plate-plate interaction, plotted as a function of the total number of bonds formed (main panel). The inset shows $U_{\rm bond,total} = \sum_n \Delta G_{\rm ij_n}$ (see text). The surface separation was fixed at $h = 1.0$ and $\Delta G^0 = -6.0\ k_{\rm B}T$. We varied $S_{\rm dna}$ and the surface area in such a way that there were always 2500 strands per plate.

into account, but unfortunately this has hardly been done so far. Also in drug design, the configurational entropy cost and combinatorial entropy gain (referred to as 'conformational entropy loss' and 'avidity entropy' in Ref.[46]) of multivalent ligand-receptor interactions have received surprisingly little attention, even though it has been recognized that these factors can strongly affect a drug's effectivity[41,42,46]. For instance, Kitov & Bundle[46] found that the combinatorial entropy gain due to multivalency of the receptors and/or ligands can completely overcome the configurational entropy cost associated with the binding of ligands that are attached to long tethers.

To clearly bring out the different entropic effects for our DNA-functionalized flat plates we compare in Fig. 3a the hybridization free energy of a pair of sticky ends when they are free in solution (ΔG^0) with the average 'binding free energy' per bond, $F_{\rm bond}(h) = F_{\rm plate,dna-att}(h)/n_{\rm bonds}(h)$, and with the average 'bond energy' as given by:

$$U_{\rm bond}(h) = \frac{\sum_n \Delta G_{\rm ij_n}}{n_{\rm bonds}(h)}$$

where the sum runs over all bonds formed and with $\Delta G_{\rm ij_n}$ for sticky end pair $i - j_{\rm n}$ from Eq. 1. The difference $U_{\rm bond}(h) - \Delta G^0$ then reflects the (positive) average configurational entropy cost per bond, $-T\overline{\Delta S_{\rm conf}}$, and $F_{\rm bond}(h) - U_{\rm bond}(h)$ is the (negative) average combinatorial entropy gain per bond, $-T\overline{\Delta S_{\rm combi}}$. We point out that the same considerations apply to

DNA-functionalized micro- and nano-particles (Section III C), but that we only discuss the details of the entropic effects for the case of flat plates, where the absence of curvature allows for a straightforward interpretation. In Fig. 3b, we have plotted the absolute value of each of the entropy contributions per plate-plate bond, for a number of different $\Delta G^0(T)$ values. One can clearly see the reduction in the configurational entropy cost for bond formation for small surface separations, as was discussed above, while for $h \uparrow 2\ L_{\rm dna}$ the cost diverges because $\Omega_{\rm ij}$ goes to zero (note that the last point shown is for $h = 1.99\ L_{\rm dna}$). Another important thing to note is that, per bond formed, the absolute magnitude of each of the entropic effects is of the same order as the hybridization free energy of the sticky ends when they are free in solution, $\sim 5 - 10\ k_{\rm B}T$. The effective binding strength of the sticky ends is thus significantly altered when they are tethered to a surface, but due to the opposite signs of the combinatorial and configurational contributions it is generally not *a priori* known what the net effect is. Also, the results of studies that compare the binding strength of sticky ends freely suspended in solution and tethered to particles (e.g. Ref.[47]) must depend on the grafting details, like the tether length and surface coverage, as these affect the magnitude of the different entropic effects. From Fig. 3b it appears that the configurational entropy cost per bond is quite insensitive to $\Delta G^0(T)$ and $S_{\rm dna}$ (the latter is not shown), though, suggesting that the sticky ends generally exclude binding configurations with a highly unfavorable entropy cost. This observation seems to contradict the hypothesis of Hill *et al.* that mis-aligned 'slipping' bonds can significantly increase the stability of DNA-functionalized nano-particle aggregates[48]. Although their constructs had a more flexible single-stranded tether backbone, similar configurational entropy effects should influence the interactions. Based on our results, it seems unlikely that less-favorable bonds, due to a strained binding geometry and/or base pair mismatches, play a significant role near the dissociation temperature of the aggregates. Instead of a difference in their ability to establish 'slipping' interactions, it is more likely that for distinct $5'$ to $3'$ base sequences (e.g. *GC* versus *CG* in Ref.[48]) the difference in their solution hybridization free energies[49] is the dominant cause of the different nano-particle dissociation temperatures.

The trends in the combinatorial entropy gain are best understood by considering both Fig. 3b-c and Fig. 4a-b. Fig. 4a shows how an increased surface coverage and a decreased surface separation lead to an increase in the average number of potential binding partners that is within reach of a sticky end (i.e. the number of sticky ends on the opposing surface whose

tether attachment points are within 2 $L_{\rm dna}$ of the attachment point of the sticky end of interest on the other surface). More partners means more different ways to form bonds and therefore the overall combinatorial entropy gain *per strand* in Fig. 3c becomes more negative for larger surface coverages and smaller plate separations. Note that, although the number of possible binding partners increases at smaller surface separations, there will also be more sharing of the same partners between neighboring sticky ends. Moreover, the overall fraction of strands that is bound increases for smaller separations (Fig. 4b) and, consequently, the average number of free binding partners that each sticky end 'sees' at a certain instant of time effectively goes through a maximum as a function of h in Fig. 4a. The change in the total number of bound strands also explains the h and ΔG^0 dependence of the combinatorial entropy gain *per bond*, Fig. 3b (refer to Fig. 2c for the ΔG^0 dependence of the fraction of bound strands). The more negative ΔG^0 and the smaller h, the larger the number of bonds formed and the smaller the combinatorial entropy gain per bond, despite the fact that the overall combinatorial entropy gain is larger (e.g. Fig. 3c). As a final illustration of the combinatorial contribution we plot in Fig. 5 $F_{\rm plate,dna-att}$ and $U_{\rm bond,total} = \sum_n \Delta G_{\rm ij_n}$ for the case that the surface separation, ΔG^0 and the total number of strands in the system (2500 per plate) are kept fixed and only $S_{\rm dna}$ is varied, thus changing the total number of bonds that is formed. From the inset we can see that $S_{\rm dna}$ indeed hardly affects the configurational entropy cost for bond formation, leading to a linear relationship between $U_{\rm bond,total}$ and the number of bonds formed. $F_{\rm plate,dna-att}$, on the contrary, depends non-linearly on the number of bonds, which unequivocally proves the presence of a combinatorial effect.

B. Predicting the sphere-sphere interaction: Derjaguin approximation

Using the Derjaguin (DJ) approximation[50], it is possible to obtain the interaction between two surfaces of arbitrary curvature from the known plate-plate interaction, provided that the radius of curvature is large compared to the range of the interaction. For same-size spheres of radius R at a distance of closest approach h – measured from pole to pole – the Derjaguin approximation predicts the following interaction free energy, which we can factorize into separate attractive and repulsive contributions (see Section III A 1):

$$\frac{F_{\rm sphere,total,DJ}}{k_{\rm B}T}(h) = \pi R \int_{h'}^{2\,L_{\rm dna}} \frac{F_{\rm plate,total}}{k_{\rm B}T\;L_{\rm dna}^2}(h)dh \tag{9}$$

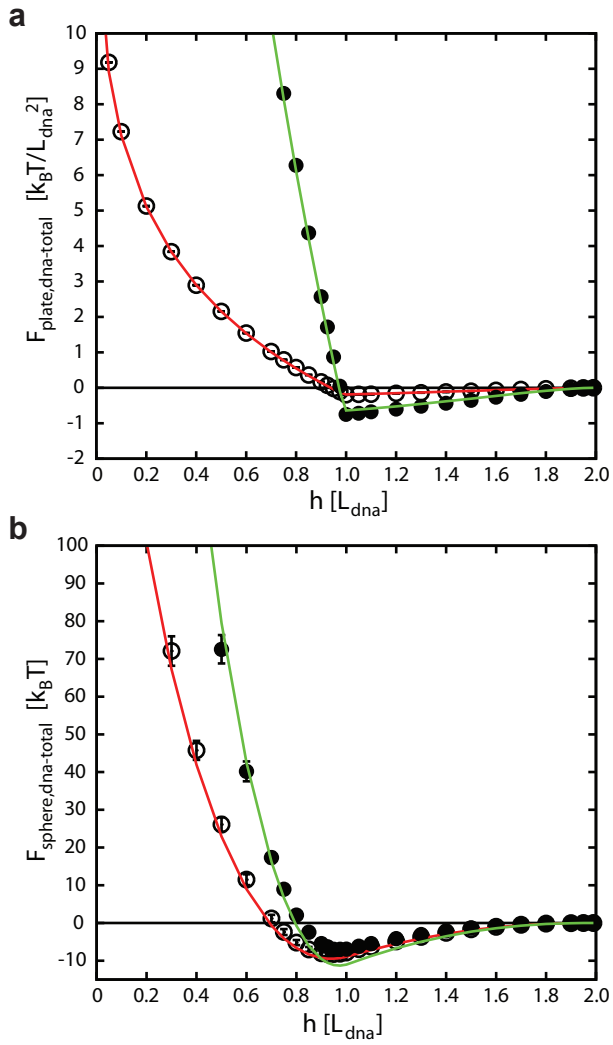

FIG. 6. Derjaguin approximation of the DNA-mediated sphere-sphere interaction. (a) Plot of our fits (solid lines) to the simulated plate-plate interaction (symbols) for $S_{\mathrm{dna}} = 0.75\ L_{\mathrm{dna}}$ / $\Delta G^0 = -6.0\ k_{\mathrm{B}}T$ (red, open symbols) and for $S_{\mathrm{dna}} = 0.25\ L_{\mathrm{dna}}$ / $\Delta G^0 = -3.0\ k_{\mathrm{B}}T$ (green, solid symbols). (b) Derjaguin approximation (solid lines) of the simulated sphere-sphere interaction (symbols) for $R = 25.0\ L_{\mathrm{dna}}$ / $S_{\mathrm{dna}} = 0.75\ L_{\mathrm{dna}}$ / $\Delta G^0 = -6.0\ k_{\mathrm{B}}T$ (red, open symbols) and for $R = 6.7\ L_{\mathrm{dna}}$ / $S_{\mathrm{dna}} = 0.25\ L_{\mathrm{dna}}$ / $\Delta G^0 = -3.0\ k_{\mathrm{B}}T$ (green, solid symbols). The error bars on the simulation data are due to the different random strand distributions of separate runs.

Obviously, $F_{\mathrm{sphere,HC,DJ}} = \infty$ when $h < 0$, reflecting the hard-core overlap of the particles (we again plot only the DNA-mediated contributions in our figures, though). We obtain the hybridization-mediated attraction, $F_{\mathrm{sphere,dna-att,DJ}}$ ($0 \leqslant h \leqslant 2\ L_{\mathrm{dna}}$), by numerically integrating the expressions for $F_{\mathrm{plate,dna-att}}$ (Eqs. 7- 8), while the confinement-induced DNA-

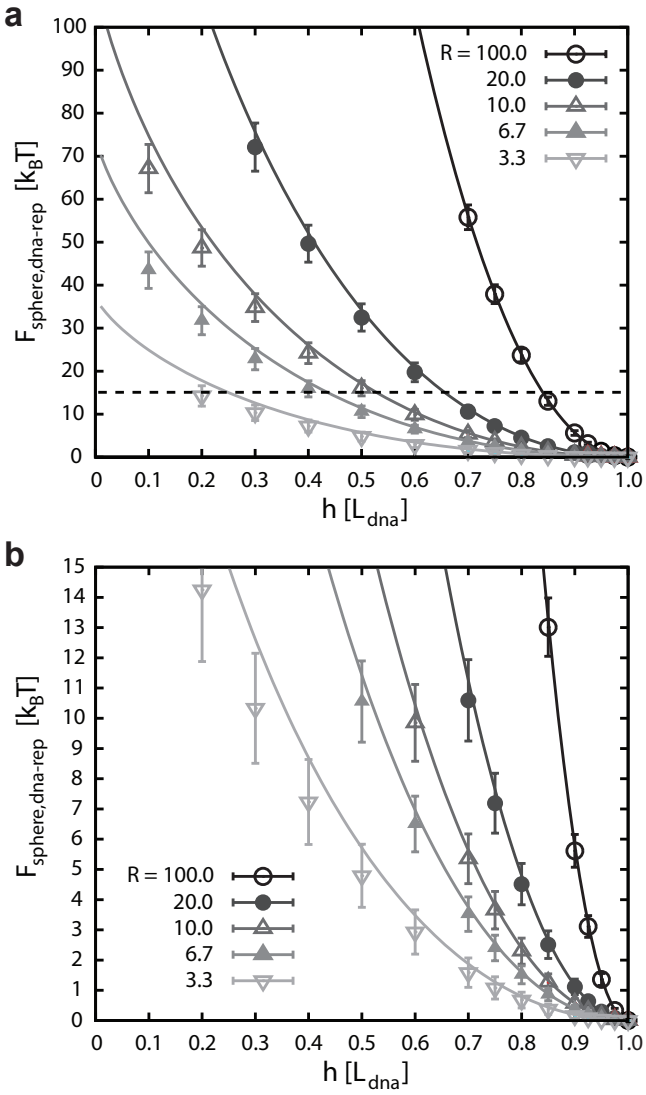

FIG. 7. Derjaguin approximation of the repulsive part of the DNA-mediated sphere-sphere interaction for $S_{\mathrm{dna}} = 0.75\ L_{\mathrm{dna}}$ and different particle sizes. (a) Solid lines: Derjaguin prediction; symbols: simulation data. (b) Close-up of the area below the dashed line in panel (a).

mediated repulsion (Eq. 5, $0 \leqslant h < L_{\mathrm{dna}}$) gives rise to the following analytical form:

$$\frac{F_{\mathrm{sphere,dna-rep,DJ}}}{k_{\mathrm{B}}T} = \frac{2\pi R}{S_{\mathrm{dna}}^2}(h \ln h - h + 1) \tag{10}$$

Note, however, that while the repulsive interaction is exactly known in the case of flat plates, there is some sphere-to-sphere variation due to their different strand distributions or, in other words, for spheres $\Omega_{\mathrm{n,confined}}$ in Eq. 3 is generally different for each of the n strands. In Fig. 6a we plot our fit to the simulated DNA-mediated plate-plate interaction for two different $\{S_{\mathrm{dna}}, \Delta G^0\}$ combinations (using the expressions derived in Section III A 1)

TABLE II. The fit constants in $F_{\mathrm{sphere,dna-rep}}$ (c_1) and $F_{\mathrm{sphere,dna-att}}$ ($c_{2,3}$), Eqs. 11- 12

c_1	-29.15
c_2	4.18×10^{-5}
c_3	-6.78×10^{-10}

and in Fig. 6b we show the corresponding Derjaguin predictions and simulation data for the pair-interaction of two spherical particle systems which will be treated in more detail in the next section. From the latter graph it appears that for the larger particles with $R = 25.0\ L_{\mathrm{dna}}$ the Derjaguin approximation performs quite well, whereas for the smaller particles with $R = 6.7\ L_{\mathrm{dna}}$ there is a clear deviation. To get a better idea of the R range in which the Derjaguin approximation gives satisfactory results we plot in Fig. 7 only the repulsive DNA-mediated interaction, because this contribution is exactly known from Eq. 10, so that any departures from the simulation data are entirely due to the finite particle curvature. As expected, the deviations are seen to increase when the particle radius becomes smaller and we find that the interaction is only well-predicted, say up to at least 50 $k_{\mathrm{B}}T$, for sphere sizes down to $R \approx 10\ L_{\mathrm{dna}}$.

C. Spheres

To extract the *pair*-interaction of same-size DNA-functionalized spheres from our computer simulations we first determine the maximum 'interaction area' on the spheres when their hard cores are in contact, i.e. the area at their poles inside which the surface-to-surface distance is maximally 2 L_{dna}. We then distribute the appropriate number of strands over these areas (again taking $L_{\mathrm{dna}} = 20$ nm), so as to obtain the desired average strand spacing, S_{dna}. The smaller the number of interacting strands, that is, the lower the coverage $1/S_{\mathrm{dna}}^2$ and the smaller the sphere radius R, the more runs with independent strand distributions are used to calculate average properties (ranging from 3 - 105 runs for our choice of parameters). For each run we use 50 equilibration and 150 production cycles. The number of trial moves is set such that in each cycle every strand is picked on average at least three times for *all* sphere-sphere separations.

1. Interaction potential

Like for planar surfaces, we can split the total sphere-sphere interaction free energy into separate hard-core repulsive ($F_{\mathrm{sphere,HC}} = \infty$ when the distance of closest approach $h < 0$) and DNA-mediated repulsive ($F_{\mathrm{sphere,dna-rep}}$) and attractive contributions ($F_{\mathrm{sphere,dna-att}}$), where we again neglect possible electrostatic contributions. We derive expressions for the DNA-mediated contributions, which are separately obtained from our simulations, by fitting the difference between the simulation data and a couple of approximate expressions for the free energy, in a way entirely analogously to the determination of $F_{\mathrm{plate,dna-att}}$ in Section III A 1. We simultaneously fit all interaction curves that correspond to a minimum in the total free energy $F_{\mathrm{sphere,total-min}} \in [-10.0, -1.0]\ k_{\mathrm{B}}T$ and with $R \in [2.5, 100.0]\ L_{\mathrm{dna}}$, $S_{\mathrm{dna}} \in [0.25, 5.00]\ L_{\mathrm{dna}}$ and $\Delta G^0 \in [-12.0, -1.0]\ k_{\mathrm{B}}T$. We fit the repulsive interaction up to 100 $k_{\mathrm{B}}T$, using a total of 12542 data points, which gives:

$$\frac{F_{\mathrm{sphere,dna-rep}}}{k_{\mathrm{B}}T}(h) = \frac{F_{\mathrm{sphere,dna-rep,DJ}}}{k_{\mathrm{B}}T}(h) + c_1 R^{-1} S_{\mathrm{dna}}^{-2} (1-h)^4 \tag{11}$$

with $F_{\mathrm{sphere,dna-rep,DJ}}$ from Eq. 10 ($0 \leqslant h < L_{\mathrm{dna}}$) and with a residual error of $\pm 0.45\ k_{\mathrm{B}}T$/point. The fitting term has the expected dependence on the surface coverage and particle size and corrects for the deviations from the Derjaguin approximation, which are increasingly important for smaller spheres, see Fig. 7. For the attractive contribution ($0 \leqslant h \leqslant 2\ L_{\mathrm{dna}}$), we find that we get the best results with the fewest fitting terms if we directly determine the correction to the Derjaguin integral of $F_{\mathrm{plate,dna-att,approx}}$ (Eq. 6), instead of using the more complex expressions for $F_{\mathrm{plate,dna-att}}$. With 19213 data points the residual error is $\pm 0.41\ k_{\mathrm{B}}T$/point and:

$$\begin{aligned}\frac{F_{\mathrm{sphere,dna-att}}}{k_{\mathrm{B}}T}(h) &= \pi R \int_{h'}^{2\ L_{\mathrm{dna}}} \frac{F_{\mathrm{plate,dna-att,approx}}}{k_{\mathrm{B}}T\ L_{\mathrm{dna}}^2}(h)dh \\ &+ \left(c_2 R S_{\mathrm{dna}}^{-4} \exp\left[-\beta\Delta G^0\right] + c_3 R S_{\mathrm{dna}}^{-6} \exp\left[-2\beta\Delta G^0\right]\right)(2-h)^3\end{aligned} \tag{12}$$

All fit constants can be found in Table II. The R dependence of the correction suggests that the deviations from the Derjaguin approximation for small spheres is fairly insignificant compared to the deviation that is introduced by the use of an approximate expression for the attractive plate-plate interaction free energy.

Taken together, the above expressions represent the simulated $F_{\mathrm{sphere,dna-total}}$ to within 10 % at all sphere separations for those combinations of $R \in [3.3, 100.0]\ L_{\mathrm{dna}}$, $S_{\mathrm{dna}} \in [0.38, 5.00]$

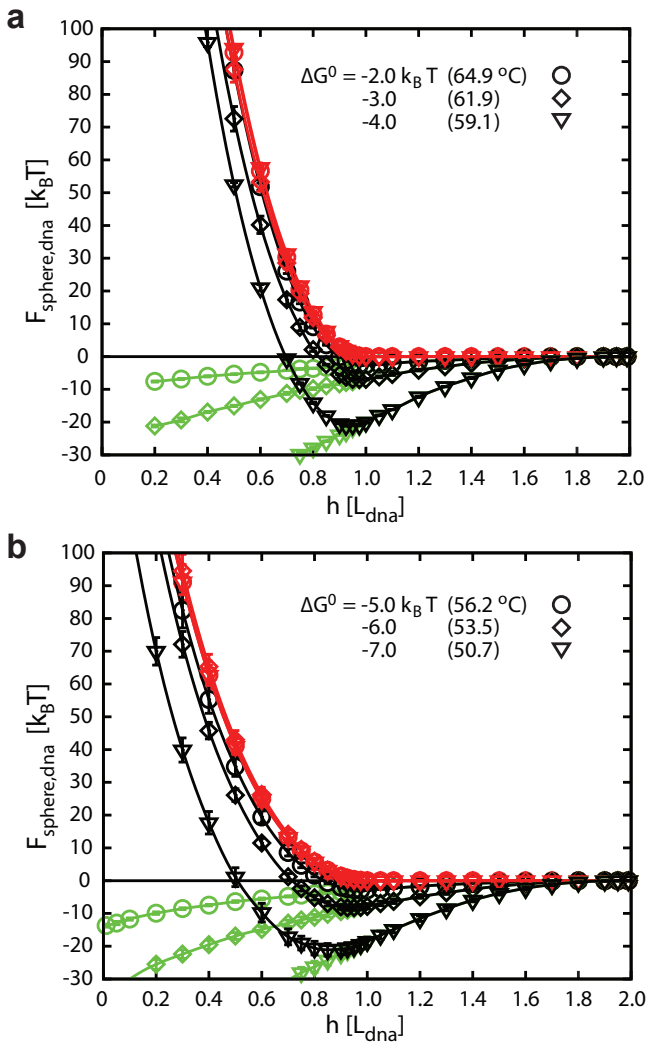

FIG. 8. The total DNA-mediated sphere-sphere interaction free energy ($F_{\mathrm{sphere,dna-total}}$, black) and the separate repulsive ($F_{\mathrm{sphere,dna-rep}}$, red) and attractive ($F_{\mathrm{sphere,dna-att}}$, green) contributions, as a function of the distance of closest approach h. (a) $R = 6.7\ L_{\mathrm{dna}}$ and $S_{\mathrm{dna}} = 0.25\ L_{\mathrm{dna}}$. (b) $R = 25.0\ L_{\mathrm{dna}}$ and $S_{\mathrm{dna}} = 0.75\ L_{\mathrm{dna}}$. The different sticky-end binding strengths (ΔG^0) used in the simulations are indicated in the panels.

L_{dna} and $\Delta G^0 \in [-12.0, -1.0]\ k_{\mathrm{B}}T$ that have a binding minimum $-10 \leqslant F_{\mathrm{sphere,total-min}} \leqslant 0\ k_{\mathrm{B}}T$ (for $R \leqslant 20.0\ L_{\mathrm{dna}}$ the S_{dna} range can be extended to $0.25\ L_{\mathrm{dna}}$). We point out that, strictly speaking, the spheres only have a purely pair-wise interaction when $R \gtrsim 6.5\ L_{\mathrm{dna}}$, if we assume that their hard cores can come into contact (otherwise the limiting radius will be smaller). For smaller radii the DNA of more than one particle can compete for the same binding partners on another particle. We expect such non-pair-wise interactions

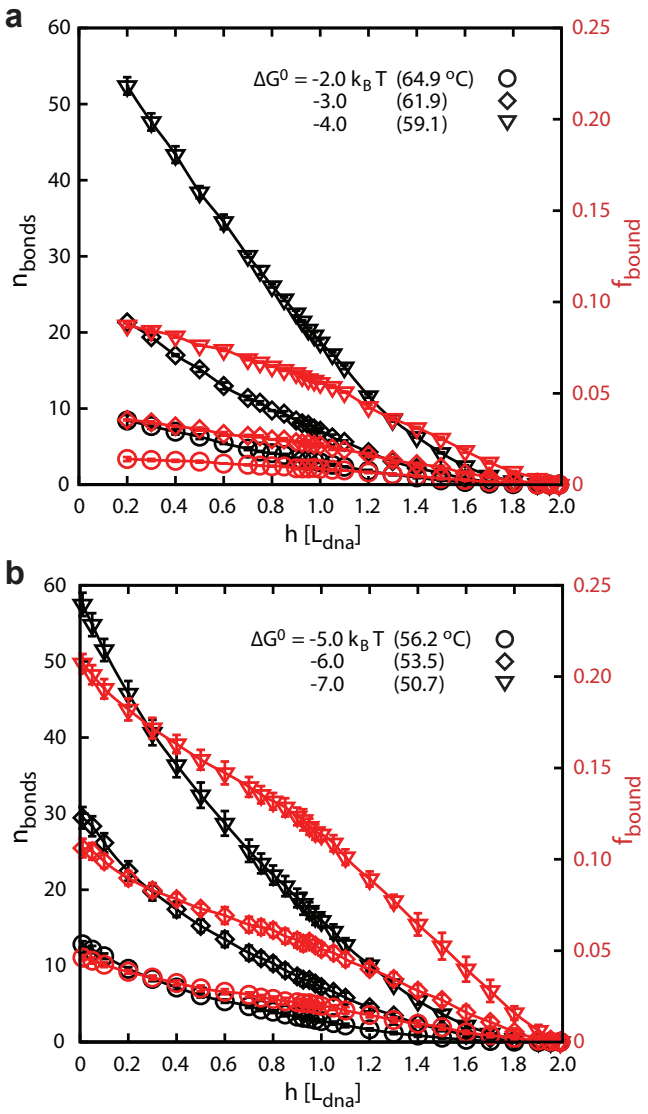

FIG. 9. The total number of bonds formed (black) and the fraction of bound sticky ends (red) as a function of the sphere separation for the same conditions as in Fig. 8a-b. (a) $R = 6.7\ L_{\rm dna}$ and $S_{\rm dna} = 0.25\ L_{\rm dna}$. (b) $R = 25.0\ L_{\rm dna}$ and $S_{\rm dna} = 0.75\ L_{\rm dna}$.

to play a role in many DNA-functionalized nano-particle systems, which frequently have $R \approx 0.5\ L_{\rm dna}$ or even less (e.g. in Refs.[10,11,23]). Instead of trying to approximate this regime, we include in Fig. 8a a graph of the DNA-mediated free energy contributions for the smallest particles in our simulations for which the interactions are still strictly pair-wise additive ($R = 6.7\ L_{\rm dna}$), at a surface coverage that is comparable to that used in some of the nano-particle experiments ($S_{\rm dna} \approx 0.25\ L_{\rm dna}$). The other graph, in Fig. 8b, is representative of some typical experimental systems of micrometer-sized colloidal particles

(e.g. Refs.[14,16,27]), where we take $R = 25.0\ L_{\rm dna}$ and $S_{\rm dna} = 0.75\ L_{\rm dna}$. Compared to the total DNA-mediated plate-plate interaction in Fig. 2a, the curves for $F_{\rm sphere,dna-total}$ have a much more pronounced attractive minimum. This is, because in the case of spheres the effective interaction area and, thereby, the number of interacting sticky ends, increases when the surface separation is decreased, whereas for plates these are essentially constant. For spheres, this does not only lead to more repulsion when the surface separation drops below $h = 1$, but also to significantly more bonds, even if the *fraction* of strands that is bound does not increase much, Fig. 9a-b. The other point to note is that the attractive minimum has a very strong temperature dependence: with the $\Delta H^0_{\rm dna}$ and $\Delta S^0_{\rm dna}$ values from Ref.[27] a change of only $\sim 3\ ^\circ C$ (corresponding to a change in ΔG^0 of about 1 $k_{\rm B}T$) can lead to a change in $F_{\rm sphere,total-min}$ of more than 10 $k_{\rm B}T$. This agrees with the sharp dissociation transitions observed in experiments[8,17,22,27,29], which are also seen if no 'cooperative melting'[51] of the bonds can occur. A simple physical argument by one of the present authors (and reproduced in Ref.[21]) qualitatively shows that the dissociation transition will become sharper as the maximum number of inter-particle bonds N increases. Namely, if the free energy difference between the bound and the unbound state of a pair of sticky ends is Δg, then the probability that a *single* pair of sticky ends is not bound is $P_{\rm u}(1) = 1/(1+\exp\left[-\beta\Delta g\right])$. If we assume that every sticky end on a particle can bind to only one particular partner strand on the opposing particle, and that each of these sticky-end pairs has the same binding strength Δg, then the probability that *all* the sticky ends between the particles are unbound is $P_{\rm u}(N) = P_{\rm u}(1)^N$. Hence, whereas $P_{\rm u}(1)$ follows a Langmuir-like curve, $P_{\rm u}(N)$ is much sharper and approaches a step function when $N \to \infty$. If the maximum possible number of inter-particle bonds is large the particles only dissociate when the probability to form a given bond is already very small, that is, when $\exp\left[-\beta\Delta g\right] \ll 1$. In this case $P_{\rm u}(N) = P_{\rm u}(1)^N \approx \exp\left[-Ne^{-\beta\Delta g}\right]$. If we assume that Δg varies linearly with T, then we can write $\Delta g \approx -\Delta s\Delta T$, with $\Delta T \equiv T - T_{\rm m}$ and $T_{\rm m}$ the temperature where $\Delta g = 0$. At $T_{\rm m}$ there is a 50% probability that a bond that can form, will form. But above $T_{\rm m}$, the unbound state is more likely than the bound state. When $\beta\Delta g \gg 1$, we obtain:

$$P_{\rm u}(N) \approx \exp\left[-Ne^{\beta\Delta s\Delta T}\right] \tag{13}$$

Thus, when the number of bonds N is not too small, the dissociation probability of a pair of particles depends doubly exponentially on the temperature. It further follows that the

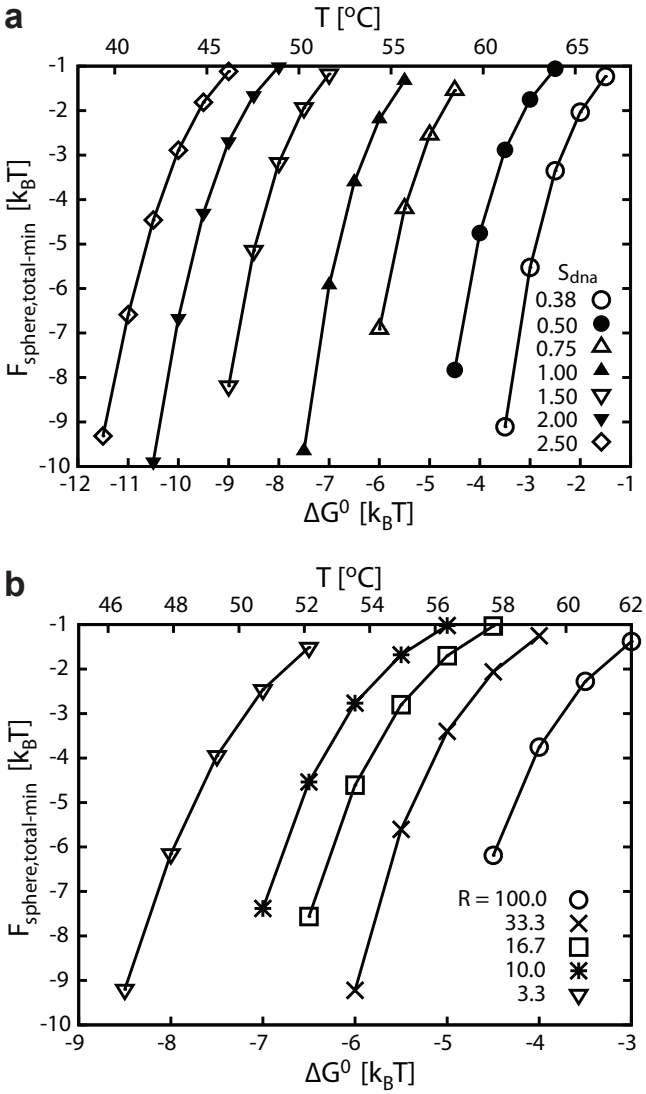

FIG. 10. The minimum sphere-sphere interaction free energy in the attractive potential well, as a function of the binding strength of the sticky ends (ΔG^0). (a) For particles with $R = 25.0\ L_{\rm dna}$ and different surface coverages. (b) For $S = 0.75\ L_{\rm dna}$ and different particle sizes.

dissociation temperature of the particles depends logarithmically on N.

2. Phase behavior

Two major determinants for the phase behavior that results from the DNA-mediated particle interactions are the depth of the attractive minimum and the range of the interaction[52,53]. To get a first impression of these interaction characteristics we plot in Fig. 10a-b the value of $F_{\rm sphere,total-min}$ as a function of ΔG^0, for a fixed particle radius and a varying coverage, as

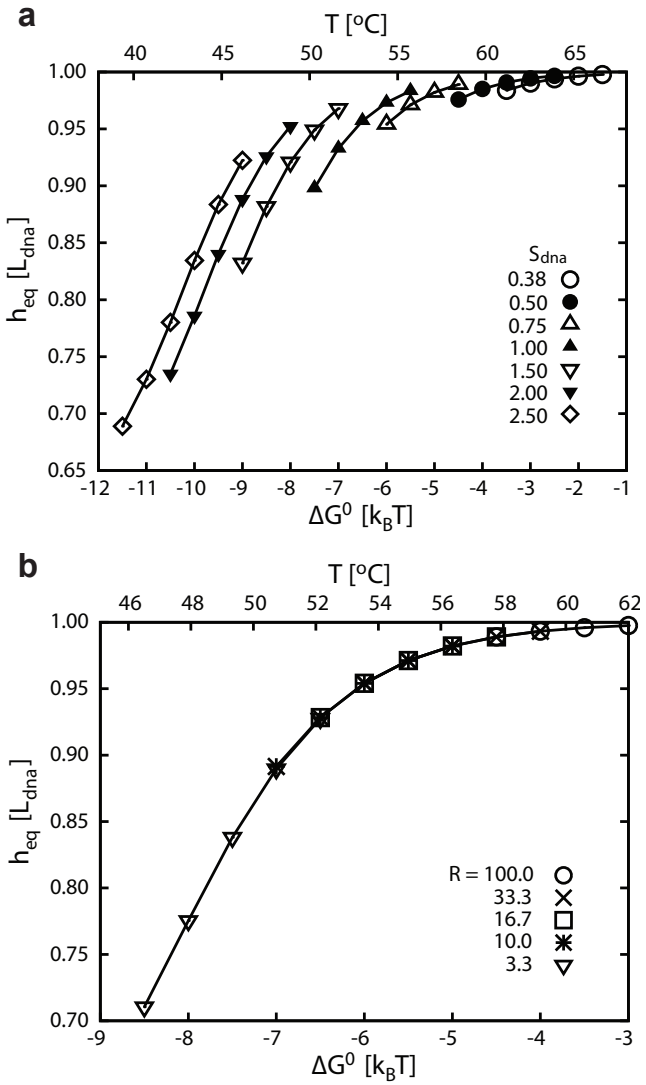

FIG. 11. The equilibrium sphere-sphere binding distance as a function of ΔG^0, at the same conditions as in Fig. 10a-b. (a) For particles with $R = 25.0\ L_{\rm dna}$ and different surface coverages. (b) For $S = 0.75\ L_{\rm dna}$ and different particle sizes.

well as for a fixed surface coverage and several different particle radii (assuming pair-wise interactions for all R and limiting ourselves to $F_{\rm sphere,total-min} \in [-10, -1]\ k_{\rm B}T$). In Fig. 11a-b we do something similar for the location of the attractive minimum, or, the equilibrium binding distance, $h_{\rm eq}$. Not surprisingly, the attractive minimum at a certain ΔG^0 is deeper for higher surface coverage (smaller $S_{\rm dna}$) and larger particle radius, because more sticky ends are available for binding in the contact area between the two surfaces. One can also recognize the strong temperature / ΔG^0 dependence of $F_{\rm sphere,total-min}$ and the crossover to a nearly linear regime at low temperatures when the number of bonds formed levels

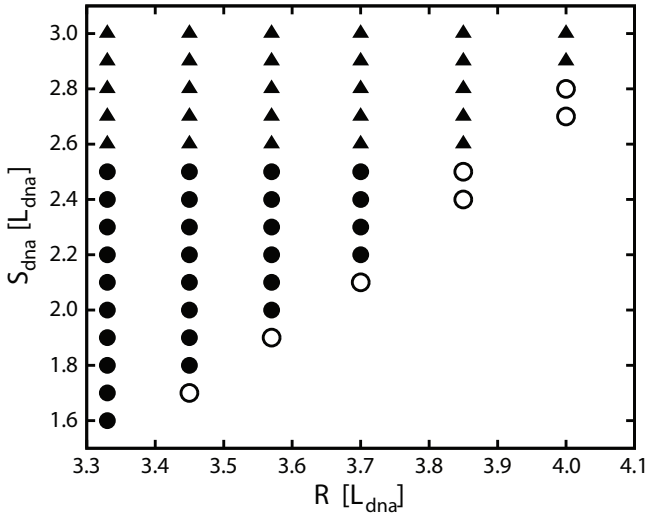

FIG. 12. Selection of $\{R, S_{\rm dna}\}$ combinations for which there is a range of ΔG^0 values (given in Tables III-IV) where the range of the interaction satisfies $r_{\rm a} \geqslant 0.13$ (see text). Open circles: reduced second virial coefficient $B_2^* > -1.5$; closed circles: $B_2^* \leqslant -1.5$; triangles: ΔG^0 outside the working range of our expressions for $F_{\rm sphere,dna-total}$ (see Section III C 1), but likely $B_2^* \leqslant -1.5$. For larger R values than those shown here the range of the interaction is $r_{\rm a} < 0.13$.

TABLE III. Characteristics of the particle-particle interaction for the data points in Fig. 12. For each $\{R, S_{\rm dna}\}$ combination the lower and upper ΔG^0 bound (in the range [-12.0, -1.0] $k_{\rm B}T$) with $r_{\rm a} \geqslant 0.13$ and $B_2^* > -1.5$ are given.

R [$L_{\rm dna}$]	$S_{\rm dna}$ [$L_{\rm dna}$]	ΔG^0 [$k_{\rm B}T$]	$r_{\rm a}$	B_2^*	$F_{\rm sphere,total-min}$ [$k_{\rm B}T$]
4.00	2.7	-10.7 / -11.5	0.13	0.62 / 0.07	-0.64 / -1.16
4.00	2.8	-10.5 / -12.0	0.13	0.74 / -0.37	-0.47 / -1.44
3.85	2.4	-10.3 / -11.3	0.13	0.59 / -0.38	-0.68 / -1.45
3.85	2.5	-10.1 / -11.8	0.13	0.73 / -1.07	-0.49 / -1.77
3.70	2.1	-10.3 / -10.7	0.13	0.20 / -0.38	-1.06 / -1.44
3.57	1.9	-10.0 / -10.6	0.13	0.08 / -1.22	-1.16 / -1.83
3.45	1.7	-10.0 / -10.1	0.13	-0.82 / -1.14	-1.67 / -1.80

off, similar to the case of planar surfaces shown in Fig. 2b-c. The number of bonds does not become entirely constant however, because the equilibrium binding distance decreases slightly with the temperature (Fig. 11), thereby bringing more sticky ends into contact.

TABLE IV. Characteristics of the particle-particle interaction for the data points in Fig. 12. For each $\{R, S_{\mathrm{dna}}\}$ combination the lower and upper ΔG^0 bound (in the range [-12.0, -1.0] $k_{\mathrm{B}}T$) with $r_{\mathrm{a}} \geqslant 0.13$ and $B_2^* \leqslant -1.5$ are given.

R [L_{dna}]	S_{dna} [L_{dna}]	ΔG^0 [$k_{\mathrm{B}}T$]	r_{a}	B_2^*	$F_{\mathrm{sphere,total-min}}$ [$k_{\mathrm{B}}T$]
3.70	2.2	-11.4	0.13	-1.70	-2.00
3.70	2.3	-11.6 / -12.0	0.13	-1.67 / -4.55	-1.97 / -2.65
3.70	2.4	-11.8 / -12.0	0.13	-1.69 / -2.79	-1.96 / -2.27
3.70	2.5	-12.0	0.13	-1.76	-1.96
3.57	2.0	-11.0 / -11.2	0.13	-1.85 / -2.89	-2.03 / -2.32
3.57	2.1	-11.2 / -11.9	0.13	-1.73 / -10.06	-1.97 / -3.30
3.57	2.2	-11.4 / -12.0	0.13	-1.66 / -7.57	-1.93 / -3.02
3.57	2.3	-11.6 / -12.0	0.14 / 0.13	-1.63 / -4.39	-1.90 / -2.56
3.57	2.4	-11.8 / -12.0	0.14	-1.65 / -2.71	-1.89 / -2.19
3.57	2.5	-12.0	0.14	-1.72	-1.90
3.45	1.8	-10.5 / -10.9	0.13	-1.74 / -4.33	-1.98 / -2.61
3.45	1.9	-10.7 / -11.7	0.13	-1.57 / -19.55	-1.90 / -3.90
3.45	2.0	-11.0 / -11.9	0.14 / 0.13	-1.82 / -19.59	-1.96 / -3.88
3.45	2.1	-11.2 / -12.0	0.14 / 0.13	-1.71 / -13.81	-1.90 / -3.53
3.45	2.2	-11.4 / -12.0	0.14	-1.64 / -7.27	-1.86 / -2.93
3.45	2.3	-11.6 / -12.0	0.14	-1.61 / -4.26	-1.84 / -2.47
3.45	2.4	-11.8 / -12.0	0.15 / 0.14	-1.62 / -2.65	-1.83 / -2.12
3.45	2.5	-12.0	0.15	-1.69	-1.83
3.33	1.6	-10.0 / -10.4	0.13	-1.78 / -4.73	-2.00 / -2.67
3.33	1.7	-10.2 / -11.2	0.13	-1.52 / -16.79	-1.88 / -3.76
3.33	1.8	-10.5 / -11.7	0.14 / 0.13	-1.73 / -46.40	-1.92 / -4.72
3.33	1.9	-10.7 / -11.8	0.14 / 0.13	-1.56 / -28.06	-1.84 / -4.19
3.33	2.0	-11.0 / -11.9	0.14 / 0.13	-1.81 / -18.59	-1.90 / -3.77
3.33	2.1	-11.2 / -12.0	0.15 / 0.14	-1.70 / -13.19	-1.84 / -3.43
3.33	2.2	-11.4 / -12.0	0.15 / 0.14	-1.62 / -7.03	-1.80 / -2.84
3.33	2.3	-11.6 / -12.0	0.15	-1.59 / -4.15	-1.78 / -2.40
3.33	2.4	-11.8 / -12.0	0.15	-1.60 / -2.60	-1.77 / -2.05
3.33	2.5	-12.0	0.1627	-1.66	-1.78

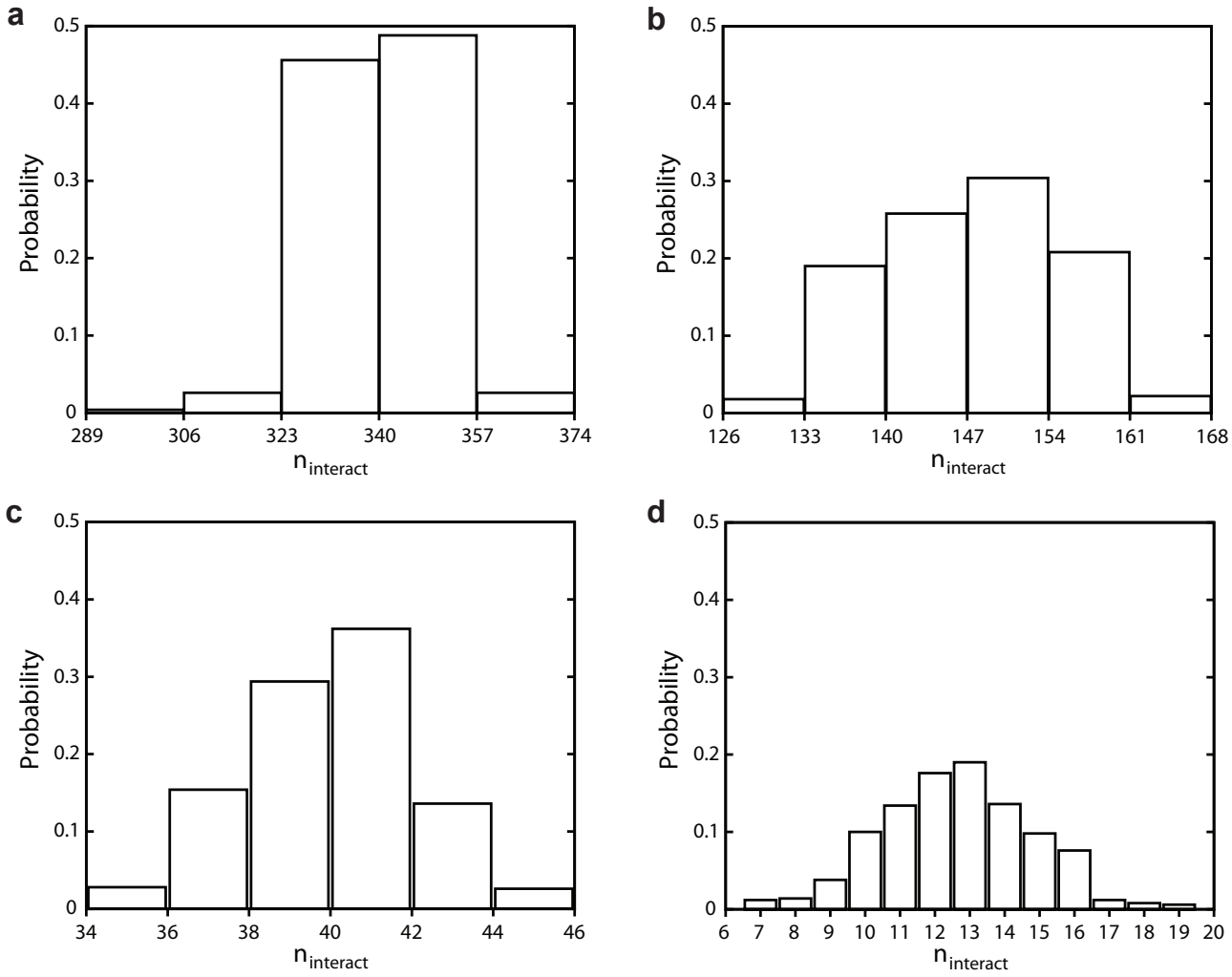

FIG. 13. Probability distribution of the number of sticky ends in the interaction area on each of the particle surfaces. (a) For $R = 6.7\ L_{\rm dna}$, $S_{\rm dna} = 0.25\ L_{\rm dna}$ and $h = 0.98\ L_{\rm dna}$ (corresponding to the curve for $\Delta G^0 = -3.0\ k_{\rm B}T$ in Fig. 8a). Each bin corresponds to a 5.0 % deviation from the mean value of $n_{\rm interact}$. (b) For $R = 25.0\ L_{\rm dna}$, $S_{\rm dna} = 0.75\ L_{\rm dna}$ and $h = 0.95\ L_{\rm dna}$ (corresponding to the curve for $\Delta G^0 = -6.0\ k_{\rm B}T$ in Fig. 8b); 4.8 % deviation per bin. (c) For $R = 0.5\ L_{\rm dna}$, $S_{\rm dna} = 0.2\ L_{\rm dna}$, $h = 1.0\ L_{\rm dna}$, $L_{\rm dna} = 15$ nm and 5.1 % deviation per bin. (d) For $R = 0.7\ L_{\rm dna}$, $S_{\rm dna} = 0.4\ L_{\rm dna}$, $h = 1.0\ L_{\rm dna}$, $L_{\rm dna} = 10$ nm and 7.9 % deviation per bin.

From Fig. 11a-b we further see that for the same range of $F_{\rm sphere,total-min} \in [-10, -1]\ k_{\rm B}T$ the equilibrium binding distance is smaller for lower coverage (larger $S_{\rm dna}$) and for smaller particles, as fewer strands contribute to the DNA-mediated repulsion.

In order to estimate the form of the phase diagram and, in particular, the stability region of the gas-liquid separation, we follow the procedure of Ref.[53] to compute the range

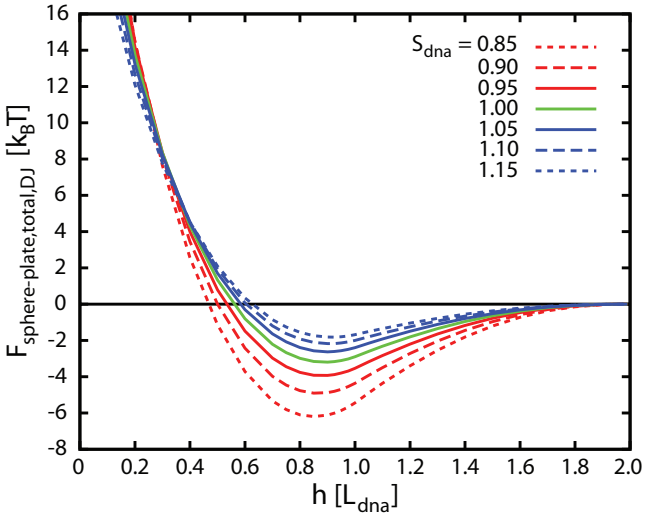

FIG. 14. Derjaguin approximation of the DNA-mediated sphere-plate interaction for $R = 4.0\ L_{\mathrm{dna}}$, $\Delta G^0 = -7.2\ k_{\mathrm{B}}T$ and several surface coverages around $S_{\mathrm{dna}} = 1.00\ L_{\mathrm{dna}}$ (red: higher coverage; blue: lower coverage).

(r_{a}) of the interaction, as given by $F_{\mathrm{sphere,total}}$, and the reduced second virial coefficient $B_2^* = B_2/B_{2,\mathrm{HS}(\sigma_{\mathrm{eff}})}$ (here, $B_{2,\mathrm{HS}(\sigma_{\mathrm{eff}})}$ is the second virial coefficient of hard spheres with a diameter equivalent to the repulsive part of our interaction). The results are given in Fig. 12 and Tables III-IV, where we have limited the calculation to $R \geqslant 3.33\ L_{\mathrm{dna}}$, $S_{\mathrm{dna}} \leqslant 3.0\ L_{\mathrm{dna}}$ and $\Delta G^0 \geqslant -12.0\ k_{\mathrm{B}}T$ (note, however, that there may be deviations from the pair-interaction $F_{\mathrm{sphere,total}}$ for $R < 6.5\ L_{\mathrm{dna}}$ due to many-body interactions, see also Section III C 1). Noro & Frenkel[53] found that generally the gas-liquid separation is stable when $r_{\mathrm{a}} \gtrsim 0.13 - 0.15$, while Vliegenthart & Lekkerkerker[52] noted that the critical point is usually located around $B_2^* \approx -1.5$. Using these two criteria we find that the gas-liquid separation only becomes stable for relatively small particles with $R \lesssim 3.7 - 4.0\ L_{\mathrm{dna}}$ and that the stability region extends to higher coverages (smaller S_{dna}) for smaller particles, although for our parameter range the coverage is still fairly low, $S_{\mathrm{dna}} \gtrsim 1.6\ L_{\mathrm{dna}}$ (Fig. 12). Clearly, in most of the experiments on colloidal particles with radii of several hundreds of nanometers the gas-liquid separation will be metastable, because the DNA-mediated interaction is very short-ranged. This agrees with the simulations of Scarlett *et al.*[38], who consistently obtained a metastable fluid phase for particle sizes and interaction strengths that correspond to the experimental systems of Ref.[37]. In contrast, many nano-particle experiments, typically with $R < L_{\mathrm{dna}}$, are performed in a regime where there should be gas-

liquid coexistence. In future work we will investigate in detail how this difference between micro- and nano-particles affects their crystallization, and other self-assembly processes. In other systems it has for instance been observed that gas-liquid separation can enhance crystal nucleation, whereas in still other cases gelation was found to interfere[54]. We point out that the possibility of a stable gas-liquid transition in nano-particle systems for sufficiently long-ranged interactions qualitatively agrees with the experiments of Macfarlane *et al.*[55], without the need to consider additional kinetic effects. Namely, these researchers observed the formation of dense disordered 'aggregates' followed by their transformation into well-ordered crystallites when they used long linkers to tether the sticky ends to the particle surface, while short linkers led to no observable intermediates between the unbound particles and crystallites. In general, the interpretation of the experimentally observed suspension behavior as a function of the linker length (e.g. the studies in Refs.[11,23]) may not be so straightforward, however, if one does not determine the exact form of the DNA-mediated interactions. For instance, as the linker length is varied not only the range of the interaction changes, but also the configurational and combinatorial entropy contributions, and thereby the overall interaction strength (Section III A 2). As mentioned before, in the limit of extremely long linkers (comparable to the particle size), one could even cross over to a different regime, with phase transitions driven entirely by entropy[36,40]. Moreover, in experiments the 'real' phase diagram could be obscured by kinetic effects, such as delayed nucleation or arrested phase separation[54]. This may be one of the reasons that crystallization is frequently found to be more successful when the temperature is cycled, for example in Ref.[11]. Due to this complexity there clearly is still a need for more theoretical and experimental studies of DNA-mediated interactions and phase behavior.

Finally, it is important to keep in mind that the random nature of the DNA distribution on the particle surface may lead to significant variations in the particle-particle interaction, depending on their mutual orientation. To illustrate this, we construct histograms of the probability to have a certain number of sticky ends in the interaction area between two spheres for several different $\{R, S_{\rm dna}\}$ combinations (at the known $h_{\rm eq}$ or, otherwise, $h = 1\ L_{\rm dna}$). Fig. 13a-b correspond to the systems with the interaction potentials of Fig. 8a-b, whereas Fig. 13c-d were drawn up for typical nano-particle parameters. Apparently, for small particles and/or low coverages there can be a wide spread in the number of interacting sticky ends; for the case of Fig. 13d the spread even is more than 50 % for the

majority of the particle encounters. If the objective is to obtain bulk crystallization this may not be too problematic, as only encounters with a sufficiently strong interaction will lead to nucleation and growth, but if the particles are used as probes for the detection of specific DNA target sequences[56] it may lead to ambiguous results. One format for such a detection assay uses DNA-functionalized nano-particles as the probes, which interact with a flat surface functionalized with single-stranded target sequences, see for example Refs.[57,58]. From the Derjaguin approximation it follows that $F_{\mathrm{sphere-plate,total,DJ}} = 2F_{\mathrm{sphere,total,DJ}}$ and using Eq. 9 we find the example curves in Fig. 14. Here, we use $R = 4\ L_{\mathrm{dna}}$ as the smallest particle size without many-body interactions in the sphere-plate geometry, and we choose ΔG^0 such that $F_{\mathrm{sphere,total-min}} \approx -3\ k_{\mathrm{B}}T$ for $S_{\mathrm{dna}} = 1.0\ L_{\mathrm{dna}}$. The steps of 0.05 L_{dna} then correspond roughly to a $\sim$10 % variation in the surface coverage, which, according to Fig. 13, is quite feasible. It can be seen that just a 10 % variation can already lead to ~ 1 $k_{\mathrm{B}}T$ change in $F_{\mathrm{sphere,total-min}}$, which can make the difference between a bound or a free nano-particle probe in the detection assay.

IV. TECHNICAL SUMMARY

The pair-interaction potentials derived here apply to solid surfaces functionalized with relatively short and stiff DNA constructs, that behave like 'rigid rods'. We provide separate expressions for the repulsive and attractive contributions to the DNA-mediated interaction, where we ignore direct strand-strand interactions of steric or electrostatic nature. For typical experimental surface coverages and ionic strengths, the repulsion due to self-avoidance is expected to be small, while the electrostatic interactions are strongly screened. Thus, only at high grafting densities would the present approach need to be refined. For planar surfaces the confinement-induced DNA-mediated repulsion, $F_{\mathrm{plate,dna-rep}}$, is given per unit area by Eq. 5, which is valid for all L_{dna}, all strand spacings S_{dna} and all plate separations $0 \leqslant h < L_{\mathrm{dna}}$. The DNA-mediated attraction, $F_{\mathrm{plate,dna-att}}$, per unit area of the planar surfaces is given by the combination of Eq. 6 with, respectively, Eq. 7 ($0 \leqslant h < 1$) and Eq. 8 ($1 \leqslant h \leqslant 2$), plus the fit constants from Table I. These expressions were derived for $L_{\mathrm{dna}} = 20$ nm and describe all $F_{\mathrm{plate,dna-att}}$ profiles that correspond to a minimum in the *total* free energy $F_{\mathrm{plate,total-min}} \in [-2.00, -0.01]\ k_{\mathrm{B}}T/L_{\mathrm{dna}}^2$ and with $S_{\mathrm{dna}} \in [0.25, 5.00]\ L_{\mathrm{dna}}$ and $\Delta G^0 \in [-12.0, -1.0]\ k_{\mathrm{B}}T$. The total DNA-mediated interaction free energy for planar surfaces, $F_{\mathrm{plate,dna-total}}$, follows

directly from the summation of the separate attractive and repulsive contributions. For spherical particles the DNA-mediated repulsion, $F_{\mathrm{sphere,dna-rep}}$, is given by the combination of Eq. 10 and Eq. 11, for $h < L_{\mathrm{dna}}$ and repulsions up to 100 $k_{\mathrm{B}}T$. The DNA-mediated attraction, $F_{\mathrm{sphere,dna-att}}$, is given by the combination of Eq. 6 and Eq. 12 ($0 \leqslant h \leqslant 2\ L_{\mathrm{dna}}$), while the total interaction free energy, $F_{\mathrm{sphere,dna-total}}$, again follows from a straightforward summation. The relevant fit constants are listed in Table II. The expressions were derived for $L_{\mathrm{dna}} = 20$ nm and describe the interactions well for those combinations of particle radii $R \in [3.3, 100.0]\ L_{\mathrm{dna}}$, $S_{\mathrm{dna}} \in [0.38, 5.00]\ L_{\mathrm{dna}}$ and $\Delta G^0 \in [-12.0, -1.0]\ k_{\mathrm{B}}T$ that have a binding minimum $-10 \leqslant F_{\mathrm{sphere,total-min}} \leqslant 0\ k_{\mathrm{B}}T$ (for radii $R \leqslant 20.0\ L_{\mathrm{dna}}$ the S_{dna} range can be extended to $0.25\ L_{\mathrm{dna}}$). We point out that for small sphere separations, $h < \sqrt{L_{\mathrm{dna}}^2 + R^2} - R$, some sticky ends explore a configurational space that differs from the '(truncated) hemisphere' geometry at larger separations (see Appendix A 3) and that these deviations are not captured by our simulations and analytical expressions. Furthermore, in a crowded suspension non-pair-wise interactions could start to occur when $R \gtrsim 6.5\ L_{\mathrm{dna}}$. Fortran procedures that give the pair-interaction potentials for different parameter combinations can be downloaded from http://www.amolf.nl/research/supramolecular-interactions/.

V. CONCLUSIONS

To summarize, we have derived expressions for the (non-electrostatic) repulsive and attractive contributions to the total interaction free energy of planar (Eqs. 5-8) and curved surfaces (Eqs. 11-12) with tethered DNA sticky ends, as obtained from Monte Carlo simulations (see also the summary in Section IV). The simulations were performed for relatively short ($L_{\mathrm{dna}} = 20$ nm) and stiff DNA constructs and our expressions capture the dependence of the resulting interactions on the DNA grafting density, the size of the particles and the (temperature-dependent) binding strength of the sticky ends. The particle size range covered extends from several tens of nanometers to a few micrometers in radius, whereas the surface coverage ranges from very dense to rather sparse (average strand spacing $\sim$ 5 - 100 nm). We further find that the Derjaguin approximation gives a reasonable prediction of the sphere-sphere pair-interaction for particle sizes of a couple hundred nanometers and up. Our rough assessment of the phase behavior resulting from the DNA-mediated interactions qualitatively agrees with the experimental descriptions found in the literature. For instance,

due to the typically large number of inter-particle bonds, small changes in the ambient temperature are seen to lead to large changes in the depth of the attractive minimum, thus giving rise to the sharp dissociation transitions observed in experiments. We further find that gas-liquid coexistence only occurs for relatively small particles with radii of a few tens of nanometers or less, which may explain the observed differences in crystallization behavior between nano-particle systems and micrometer-sized colloids. Note, however, that kinetic effects could obscure the thermodynamic phase behavior and that more detailed studies are needed to obtain a full understanding. We have also shown that in some cases statistical non-uniformities in the DNA distribution can play an important role too, as this can lead to a significant variation in the particle interactions. Generally, this natural heterogeneity will be more pronounced for smaller particles and lower grafting densities, and one should be aware of its possible consequences in nano-particle-based DNA-detection assays. In addition, the discrete character of the tethered sticky ends has some other interesting effects, which are entropic in nature: the restricted freedom of motion of a hybridized pair of sticky ends imposes a configurational entropy cost for bond formation, whereas the multiplicity of different binding configurations for the entire ensemble of sticky ends gives rise to a combinatorial entropy gain. Both of these entropic effects depend on the grafting details, such as the tether length and the surface coverage. For the example system studied here, we find that per bond formed each of these contributions is of the same order of magnitude as the hybridization free energy of a pair of sticky ends when they are free in solution ($\sim 5-10\ k_{\mathrm{B}}T$). They thus have a strong effect on the effective binding strength of the tethered sticky ends, but due to their opposite sign it is not always straightforward what their net effect will be if one does not calculate the full interactions. We conclude by pointing out that our results do not only further the understanding of the microscopic interactions and phase behavior in systems of DNA-functionalized micro- and nano-particles, but that they are also relevant in chemical or biological contexts, such as supramolecular self-assembly or ligand-receptor mediated bio-recognition. It is actually surprising that the entropic effects highlighted above have received very little attention so far, because tethered binding groups are increasingly used to engineer the interactions in, for instance, biosensing and self-assembling micro- and nanostructured materials, while multivalent interactions have been found to be a potentially very powerful tool when it comes to targeted drug delivery or the inhibition/promotion of certain biological interactions and cellular responses.

Appendix A: Hybridization free energy of tethered DNA

1. Configurational entropy cost

We can derive an expression for the hybridization free energy of a complementary pair $i-j$ of tethered DNA sticky ends, which includes an additional configurational entropy cost, by comparing with the hybridization equilibrium of the DNA when it is free in solution. Assuming a negligible change in the reaction pressure and volume upon hybridization, the hybridization free energy is given by:

$$\Delta G_{\mathrm{ij}} = -k_{\mathrm{B}}T \ln\left(\frac{Z_{\mathrm{ij}}}{Z_{\mathrm{i}}Z_{\mathrm{j}}}\right) \tag{A1}$$

where $Z_{\mathrm{i,j,ij}}$ represents the partition function $Z_{\mathrm{N,V,T}} = \Omega^N z_{\mathrm{int}}^N/\Lambda^{dN}N!$ of N molecules of the unhybridized species i / j or the hybridized species ij, respectively. Here, Ω is the 'configurational space' of the species under consideration, d is the dimensionality of this space, and $\Lambda_{\mathrm{i,j,ij}} = \sqrt{h_{\mathrm{P}}^2/2\pi m_{\mathrm{i,j,ij}}k_{\mathrm{B}}T}$ is the thermal De Broglie wavelength (h_{P} is Planck's constant and $m_{\mathrm{i,j,ij}}$ is the mass of the respective species). z_{int} represents the contribution to the partition function due to all internal degrees of freedom. For a single pair of sticky ends we can write:

$$\frac{Z_{\mathrm{ij}}}{Z_{\mathrm{i}}Z_{\mathrm{j}}} = \frac{\Omega_{\mathrm{ij}}}{\Omega_{\mathrm{i}}\Omega_{\mathrm{j}}}\frac{z_{\mathrm{int,ij}}/\Lambda_{\mathrm{ij}}^{d_{\mathrm{ij}}}}{z_{\mathrm{int,i}}z_{\mathrm{int,j}}/\Lambda_{\mathrm{i}}^{d_{\mathrm{i}}}\Lambda_{\mathrm{j}}^{d_{\mathrm{j}}}}} \tag{A2}$$

From Fig. 1a it is clear that for tethered sticky ends $\Omega_{\mathrm{ij}} \neq \Omega_{\mathrm{i,j}}$, while for sticky ends in solution $\Omega_{\mathrm{ij}} = \Omega_{\mathrm{i,j}} = V$. For the sticky ends in solution we know the equilibrium constant:

$$K_{\mathrm{eq,ij}} = \frac{[ij]}{[i][j]} = \exp[-\beta\Delta G^0_{\mathrm{ij,solution}}] \tag{A3}$$

Here, $[x] = \rho_{\mathrm{x}}/\rho^0$, with $\rho = N/V$ and ρ^0 the standard number density. Using $F = -k_{\mathrm{B}}T\ln(Z_{\mathrm{N,V,T}})$, the chemical potential $\mu = \left(\frac{\partial F}{\partial N}\right)_{\mathrm{P,T}}$ and the equilibrium condition $\mu_{\mathrm{i}}+\mu_{\mathrm{j}} = \mu_{\mathrm{ij}}$ to derive an expression for $\rho_{\mathrm{ij}}/\rho_{\mathrm{i}}\rho_{\mathrm{j}}$, we find by combining with Eq. A3 that:

$$\frac{z_{\mathrm{int,ij}}/\Lambda_{\mathrm{ij}}^3}{z_{\mathrm{int,i}}z_{\mathrm{int,j}}/\Lambda_{\mathrm{i}}^3\Lambda_{\mathrm{j}}^3} = \frac{K_{\mathrm{eq,ij}}}{\rho^0} \tag{A4}$$

If we assume that z_{int} does not change when the sticky ends are tethered to a surface, we can combine Eqs. A1, A2 and A4 to obtain the following expression for the hybridization

free energy of a pair of tethered sticky ends:

$$\Delta G_{\mathrm{ij,tether}} = -k_{\mathrm{B}}T \ln\left(\frac{\Omega_{\mathrm{ij}}}{\Omega_{\mathrm{i}}\Omega_{\mathrm{j}}}\frac{\Lambda_{\mathrm{ij}}^{3-d_{\mathrm{ij}}}}{\Lambda_{\mathrm{i}}^{3-d_{\mathrm{i}}}\Lambda_{\mathrm{j}}^{3-d_{\mathrm{j}}}}\frac{K_{\mathrm{eq,ij}}}{\rho^0}\right) = \Delta G^0_{\mathrm{ij,solution}} - k_{\mathrm{B}}T \ln\left(\frac{\Omega_{\mathrm{ij}}}{\Omega_{\mathrm{i}}\Omega_{\mathrm{j}}}\frac{\Lambda_{\mathrm{ij}}^{3-d_{\mathrm{ij}}}}{\Lambda_{\mathrm{i}}^{3-d_{\mathrm{i}}}\Lambda_{\mathrm{j}}^{3-d_{\mathrm{j}}}}\frac{1}{\rho^0}\right) \tag{A5}$$

$$= \Delta G^0_{\mathrm{ij,solution}} - T\Delta S_{\mathrm{conf}}$$

where ΔS_{conf} is the configurational entropy cost upon hybridization and the $\Omega_{\mathrm{i,j,ij}}$ now represent the configurational space of the tethered sticky ends. For our rod-like DNA constructs $d_{\mathrm{i,j}} = 2$, $d_{\mathrm{ij}} = 1$ and $\Lambda_{\mathrm{ij}}^{3-d_{\mathrm{ij}}}/\Lambda_{\mathrm{i}}^{3-d_{\mathrm{i}}}\Lambda_{\mathrm{j}}^{3-d_{\mathrm{j}}} = \frac{1}{2}$, which effectively adds a small constant offset that is independent of the particular pair of sticky ends under consideration, but which we neglect in our calculations. Below, we derive expressions for $\Omega_{\mathrm{i,j,ij}}$ for the case of two flat plates or two same-size spheres interacting with each other.

2. Plate-plate geometry

a. Unhybridized sticky ends ($\Omega_{\mathrm{i,j}}$)

If the surface-surface separation $h \geqslant L_{\mathrm{dna}}$ the tethered DNA constructs are unconfined and their sticky endpoints trace (independently of each other) the surface area of a full hemi-sphere, whereas if $h < L_{\mathrm{dna}}$ the sticky ends trace a truncated hemisphere (Fig. 1b):

$$\Omega_{\mathrm{i,j}} = \begin{cases} \Omega_{\mathrm{i,j,unconfined}} = 2\pi L_{\mathrm{dna}}^2, & h \geqslant L_{\mathrm{dna}} \\ \Omega_{\mathrm{i,j,confined}} = 2\pi h L_{\mathrm{dna}}, & h < L_{\mathrm{dna}} \end{cases}$$

b. Hybridized sticky ends (Ω_{ij})

Depending on the surface-surface separation, h, and the relative positions of the surface attachment points of the tethers, a pair of hybridized sticky ends traces the circumference of either a full or a truncated circle. If $\mathbf{r}_{\mathrm{ij}}$ is the vector connecting the attachment points of DNA constructs i and j, and we define $r_\perp$ to be the length of the projection of $\mathbf{r}_{\mathrm{ij}}$ on either surface, then:

$$\Omega_{\mathrm{ij}} = \begin{cases} \Omega_{\mathrm{ij,full}} = 2\pi\sqrt{L_{\mathrm{dna}}^2 - \frac{1}{4}(h^2 + r_\perp^2)} \\ \Omega_{\mathrm{ij,truncated}} = \left(2\pi - 4\arccos\left[\frac{h\sqrt{h^2+r_\perp^2}}{2r_\perp\sqrt{L_{\mathrm{dna}}^2 - \frac{1}{4}(h^2+r_\perp^2)}}\right]\right)\sqrt{L_{\mathrm{dna}}^2 - \frac{1}{4}(h^2 + r_\perp^2)} \end{cases}$$

The circle is truncated if $r_{\perp,1} < r_{\perp} < r_{\perp,2}$, with $r_{\perp,1,2} = \sqrt{2L_{\mathrm{dna}}^2 - h^2 \mp 2L_{\mathrm{dna}}\sqrt{L_{\mathrm{dna}}^2 - h^2}}$.

3. Sphere-sphere geometry

For same-size spheres of radius R at a distance of closest approach h (measured from pole to pole) the attachment points of DNA constructs i and j have the following coordinates:

$$\begin{aligned} x_{\mathrm{i,j}} &= R\sin\phi_{\mathrm{i,j}}\cos\theta_{\mathrm{i,j}} \\ y_{\mathrm{i,j}} &= R\sin\phi_{\mathrm{i,j}}\sin\theta_{\mathrm{i,j}} \\ z_{\mathrm{i}} &= R\cos\phi_{\mathrm{i}} \\ z_{\mathrm{j}} &= R\cos\phi_{\mathrm{j}} + 2R + h \end{aligned}$$

Here, $\phi_{\mathrm{i,j}}$ is the angle between the vector that connects the two sphere centers ($\|\mathbf{z}$) and the vector that connects the attachment point of DNA construct i / j with the center of the sphere on which the construct resides.

a. Unhybridized sticky ends ($\Omega_{\mathrm{i,j}}$)

If $h \geqslant L_{\mathrm{dna}}$ all DNA constructs are unconfined and their sticky endpoints trace the surface area of a full hemi-sphere:

$$\Omega_{\mathrm{i,j}} = \Omega_{\mathrm{i,j,unconfined}} = 2\pi L_{\mathrm{dna}}^2$$

If $h < L_{\mathrm{dna}}$ a DNA construct is only unconfined if $z_{\mathrm{i}} \leqslant z_{\mathrm{bound,i}}$ or $z_{\mathrm{j}} \geqslant z_{\mathrm{bound,j}}$, with:

$$z_{\mathrm{bound,i,j}} = \frac{\pm(R^2 - (R + L_{\mathrm{dna}})^2) + (2R + h)^2}{2(2R + h)}$$

If $h < L_{\mathrm{dna}}$ and $z_{\mathrm{i}} \geqslant z_{\mathrm{bound,i}}$ or $z_{\mathrm{j}} \leqslant z_{\mathrm{bound,j}}$ the DNA construct is confined and its sticky endpoint traces the surface area of a truncated hemi-sphere:

$$\Omega_{\mathrm{i,j}} = \Omega_{\mathrm{i,j,confined}} = 2\pi L_{\mathrm{dna}}\sqrt{L_{\mathrm{dna}}^2 - r_{\mathrm{cap}}^2}$$

with r_{cap} the radius of the circular base of the truncated cap:

$$r_{\mathrm{cap}} = R\sqrt{1 - \left(\frac{R^2 + D^2 - L_{\mathrm{dna}}^2}{2RD}\right)^2}$$

and D the length of the vector that connects the center of the opposing sphere (i.e. the sphere other than the one that the DNA construct of interest resides on) to the center of the truncated cap base:

$$D^2 = (2R + h^2) + R^2 - 2R(2R + h)\cos\alpha_{\mathrm{i,j}}$$

where $\alpha_{\mathrm{i}} = \phi_{\mathrm{i}}$ and $\alpha_{\mathrm{j}} = \pi - \phi_{\mathrm{j}}$. We point out that the geometry becomes more complex than that of a simple (truncated) hemi-sphere when $h < \sqrt{L_{\mathrm{dna}}^2 + R^2} - R$. In our simulations this typically applies to a very limited range of small sphere separations only and therefore we do not consider this case, but limit ourselves to sufficiently large h values.

b. Hybridized sticky ends (Ω_{ij})

Similar to the case of flat plates, the connected endpoints of a hybridized pair of DNA constructs $i - j$ trace the circumference of either a full or a truncated circle. The truncated 'interaction circles' are generally no longer symmetric though, due to the curvature of the surfaces and the asymmetric attachment locations of the DNA constructs. Therefore, we divide the total interaction circle into two semi-circles, 1 and 2, each of which can again be either full or truncated. Then:

$$\Omega_{\mathrm{ij}} = 2[\pi - (\beta_1 + \beta_2)]r_{\mathrm{full}}$$

where $\beta_{1,2}$ is the angle that is excluded from semi-circle 1 and 2 respectively, and where r_{full} is the radius of the interaction circle if it would not be truncated:

$$r_{\mathrm{full}} = \sqrt{L_{\mathrm{dna}}^2 - \left(\frac{|\mathbf{r}_{\mathrm{ij}}|}{2}\right)^2}$$

It can be derived that $\beta_{1,2} = \arccos(H_{1,2}/r_{\mathrm{full}})$, with $H_{1,2} = (|\mathbf{r}_{\mathrm{ij}}|/2)\tan\gamma_{1,2}$ the 'height' of the truncated semi-circles 1 and 2. Further:

$$\gamma_1 = \arccos\left(\frac{R^2 + |\mathbf{r}_{\mathrm{ij}}|^2 - x_{\mathrm{i}}^2 - y_{\mathrm{i}}^2 - (z_{\mathrm{i}} - (2R + h))^2}{2R|\mathbf{r}_{\mathrm{ij}}|}\right) - \frac{\pi}{2}$$
$$\gamma_2 = \arccos\left(\frac{R^2 + |\mathbf{r}_{\mathrm{ij}}|^2 - x_{\mathrm{j}}^2 - y_{\mathrm{j}}^2 - z_{\mathrm{j}}^2}{2R|\mathbf{r}_{\mathrm{ij}}|}\right) - \frac{\pi}{2}$$

Note that if $\tan\gamma_{1,2} \leqslant 2r_{\mathrm{full}}/|\mathbf{r}_{\mathrm{ij}}|$ that $\beta_{1,2} = 0$.

Appendix B: Thermodynamic integration

In our systems, the total partition function for the sticky end interactions is always of the form:

$$Z_{\text{total}} = \sum_{n=0}^{M} \left(\exp\left[-\beta \Delta G^0_{\text{solution}}\right]\right)^n Z_{\text{combi}}(\mathbf{n})$$

where M is the theoretical maximum of the number of bonds and n is the actual number of bonds formed, while $Z_{\text{combi}}(\mathbf{n})$ essentially reflects the number of different ways in which they can be formed between the two surfaces. Using $F = -k_{\text{B}}T \ln Z_{\text{total}}$ we get:

$$\left(\frac{\partial F}{\partial \Delta G^0}\right) = -k_{\text{B}}T \frac{1}{Z_{\text{total}}} \frac{\partial Z_{\text{total}}}{\partial \Delta G^0} = -k_{\text{B}}T \left\langle n_{\text{bonds}} \right\rangle_{\Delta \text{G}^0}$$

with $\left\langle n_{\text{bonds}} \right\rangle_{\Delta \text{G}^0}$ the average number of bonds that is formed at ΔG^0. The thermodynamic integration to obtain the interaction free energy at a particular $\Delta G^{0\prime}$ thus takes the following form:

$$\frac{F_{\text{dna-bound}}}{k_{\text{B}}T} = \frac{F_{\text{dna-unbound}}}{k_{\text{B}}T} - \int_{\Delta G^{0\prime}}^{0} \left\langle n_{\text{bonds}} \right\rangle_{\Delta \text{G}^0} d\Delta G^0$$

We point out that the upper integration limit technically is $\Delta G^0 = \infty$, but that we can truncate the calculation at ΔG^0 values that are too large for bond formation. Here, we have arbitrarily set the limit to zero, because for our systems of interest we did not observe bond formation for these or larger ΔG^0 values (see for example Fig. 2c). Note, however, that in certain other systems, for instance in bulk solutions where there is no configurational entropy cost for bond formation, a significant fraction of the DNA can be hybridized even at $\Delta G^0 \geqslant 0$. In fact, the numerical value of ΔG^0 depends on the definition of the reference state. Hence, $\Delta G^0 = 0$ has no special meaning.

Appendix C: Approximate DNA-mediated plate attraction ($F_{\text{plate,dna-att,approx}}$)

We obtain an approximate expression for the attractive contribution to the DNA-mediated plate-plate interaction free energy from $F_{\text{plate,dna-att,approx}} = -k_{\text{B}}T \ln Z_{\text{plate,dna-att,approx}}$ and the simplified partition function:

$$Z_{\text{plate,dna-att,approx}} = (1 + \overline{n}_{\text{partner}} \exp\left[-\beta \overline{\Delta G_{\text{ij}}}\right])^{N_{\text{plate}}}$$

Here, $\exp\left[-\beta \overline{\Delta G_{\text{ij}}}\right]$ is the *average* Boltzmann weight of a bound pair of sticky ends (the unbound state has weight 1) and $\overline{n}_{\text{partner}} = \pi(4L^2_{\text{dna}} - h^2)/S^2_{\text{dna}}$ is the average number of

strands j on the opposing surface that is within binding reach of a strand i. For the plate-plate geometry under consideration it follows from Eq. 1 that:

$$\overline{\Delta G_{\mathrm{ij}}} = \Delta G^0 - T\overline{\Delta S_{\mathrm{conf}}} = \Delta G^0 - k_{\mathrm{B}}T \ln\left(\frac{\overline{\Omega_{\mathrm{ij}}}}{\Omega_{\mathrm{i}}\Omega_{\mathrm{j}}\rho^0}\right)$$

with $\Omega_{\mathrm{i,j}}$ from Appendix A 2. We approximate $\overline{\Omega_{\mathrm{ij}}}$ by taking an unweighted average over the $\overline{n}_{\mathrm{partner}}$ different binding possibilities per strand:

$$\begin{aligned}\overline{\Omega_{\mathrm{ij}}} &= \frac{1}{\pi r_{\perp,\max}^2}\int_0^{r_{\perp,\max}} 2\pi r_\perp \Omega_{\mathrm{ij}} dr_\perp \\ &= \frac{2}{r_{\perp,\max}^2}\left(\int_0^{r_{\perp,1}} r_\perp \Omega_{\mathrm{ij,full}} dr_\perp + \int_{r_{\perp,1}}^{r_{\perp,2}} r_\perp \Omega_{\mathrm{ij,truncated}} dr_\perp + \int_{r_{\perp,2}}^{r_{\perp,\max}} r_\perp \Omega_{\mathrm{ij,full}} dr_\perp\right)\end{aligned}$$

with the Ω_{ij} and $r_{\perp,1,2}$ from Appendix A 2 b and with $r_{\perp,\max} = \sqrt{4L_{\mathrm{dna}}^2 - h^2}$.

ACKNOWLEDGMENTS

We thank Mark Miller for sharing his c-implementation of the Levenberg-Marquardt method with us. This work is part of the research programme of the Foundation for Fundamental Research on Matter (FOM), which is part of the Netherlands Organisation for Scientific Research (NWO). DF acknowledges financial support from the Royal Society of London (Wolfson Merit Award) and from the ERC (Advanced Grant agreement 227758).

REFERENCES

[1]S. Mann, W. Shenton, M. Li, S. Connolly, and D. Fitzmaurice, "Biologically programmed nanoparticle assembly," Advanced Materials, **12**, 147–150 (2000)

[2]A. L. Hiddessen, S. D. Rodgers, D. A. Weitz, and D. A. Hammer, "Assembly of binary colloidal structures via specific biological adhesion," Langmuir, **16**, 9744–9753 (2000)

[3]S. K. Lee, M. M. Maye, Y. B. Zhang, O. Gang, and D. Van der Lelie, "Controllable g5p-protein-directed aggregation of ssDNA-gold nanoparticles," Langmuir, **25**, 657–660 (2009)

[4]F. A. Aldaye, A. L. Palmer, and H. F. Sleiman, "Assembling materials with DNA as the guide," Science, **321**, 1795–1799 (2008)

[5]J. Zheng, J. J. Birktoft, Y. Chen, T. Wang, R. Sha, P. E. Constantinou, S. L. Ginell, C. Mao, and N. C. Seeman, "From molecular to macroscopic via the rational design of a self-assembled 3D DNA crystal," Nature, **461**, 74–77 (2009)

[6]T. Liedl, B. Hogberg, J. Tytell, D. E. Ingber, and W. M. Shih, "Self-assembly of three-dimensional prestressed tensegrity structures from DNA," Nature Nanotechnology, **5**, 520–524 (2010)

[7]K. Lund, A. J. Manzo, N. Dabby, N. Michelotti, A. Johnson-Buck, J. Nangreave, S. Taylor, R. Pei, M. N. Stojanovic, N. G. Walter, E. Winfree, and H. Yan, "Molecular robots guided by prescriptive landscapes," Nature, **465**, 206–210 (2010)

[8]C. A. Mirkin, R. L. Letsinger, R. C. Mucic, and J. J. Storhoff, "A DNA-based method for rationally assembling nanoparticles into macroscopic materials," Nature, **382**, 607–609 (1996)

[9]A. P. Alivisatos, K. P. Johnsson, X. Peng, T. E. Wilson, C. J. Loweth, M. P. Bruchez Jr, and P. G. Schultz, "Organization of 'nanocrystal molecules' using DNA," Nature, **382**, 609–611 (1996)

[10]S. Y. Park, A. K. R. Lytton-Jean, B. Lee, S. Weigand, G. C. Schatz, and C. A. Mirkin, "DNA-programmable nanoparticle crystallization," Nature, **451**, 553–556 (2008)

[11]D. Nykypanchuk, M. M. Maye, D. van der Lelie, and O. Gang, "DNA-guided crystallization of colloidal nanoparticles," Nature, **451**, 549–552 (2008)

[12]M. M. Maye, M. T. Kumara, D. Nykypanchuk, W. B. Sherman, and O. Gang, "Switching binary states of nanoparticle superlattices and dimer clusters by DNA strands," Nature Nanotechnology, **5**, 116–120 (2010)

[13]C. Niemeyer, B. Ceyhan, and P. Hazarika, "Oligofunctional DNA-gold nanoparticle conjugates," Angew. Chem. Int. Ed., **42**, 5766–5770 (2003)

[14]P. L. Biancaniello, A. J. Kim, and J. C. Crocker, "Colloidal interactions and self-assembly using DNA hybridization," Phys. Rev. Lett., **94**, 058302 (2005)

[15]P. H. Rogers, E. Michel, C. A. Bauer, S. Vanderet, D. Hansen, B. K. Roberts, A. Calvez, J. B. Crews, K. O. Lau, A. Wood, D. J. Pine, and P. V. Schwartz, "Selective, controllable, and reversible aggregation of polystyrene latex microspheres via DNA hybridization," Langmuir, **21**, 5562–5569 (2005)

[16]M. P. Valignat, O. Theodoly, J. C. Crocker, W. B. Russel, and P. M. Chaikin, "Reversible self-assembly and directed assembly of DNA-linked micrometer-sized colloids," Proc. Natl.

Acad. Sci. USA, **102**, 4225–4229 (2005)

[17]Y. Sun, N. Harris, and C. Kiang, "Melting transition of directly linked gold nanoparticle DNA assembly," Physica A, **350**, 89–94 (2005)

[18]H. Yao, C. Yi, C. Tzang, J. Zhu, and M. Yang, "DNA-directed self-assembly of gold nanoparticles into binary and ternary nanostructures," Nanotechnology, **18**, 015102 (2007)

[19]M. E. Leunissen, R. Dreyfus, R. Sha, T. Wang, N. C. Seeman, D. J. Pine, and P. M. Chaikin, "Towards self-replicating materials of DNA-functionalized colloids," Soft Matter, **5**, 2422–2430 (2009)

[20]M. E. Leunissen, R. Dreyfus, F. C. Cheong, D. G. Grier, R. Sha, N. C. Seeman, and P. M. Chaikin, "Switchable self-protected attractions in DNA-functionalized colloids," Nature Mater., **8**, 590–595 (2009)

[21]N. Geerts and E. Eiser, "DNA-functionalized colloids: Physical properties and applications," Soft Matter, DOI: 10.1039/c001603a (2010)

[22]R. Jin, G. Wu, Z. Li, C. A. Mirkin, and G. C. Schatz, "What controls the melting properties of DNA-linked gold nanoparticle assemblies?" J. Am. Chem. Soc., **125**, 1643–1654 (2003)

[23]R. J. Macfarlane, M. R. Jones, A. J. Senesi, K. L. Young, B. Lee, J. Wu, and C. A. Mirkin, "Establishing the design rules for DNA-mediated programmable colloidal crystallization," Angew. Chem. Int. Ed., **49**, 4589–4592 (2010)

[24]M. M. Maye, D. Nykypanchuk, D. Van der Lelie, and O. Gang, "A simple method for kinetic control of DNA-induced nanoparticle assembly," J. Am. Chem. Soc., **128**, 14020–14021 (2006)

[25]D. Nykypanchuk, M. M. Maye, D. van der Lelie, and O. Gang, "DNA-based approach for interparticle interaction control," Langmuir, **23**, 6305–6314 (2007)

[26]A. J. Kim, P. L. Biancaniello, and J. C. Crocker, "Engineering DNA-mediated colloidal crystallization," Langmuir, **22**, 1991–2001 (2006)

[27]R. Dreyfus, M. E. Leunissen, R. Sha, A. V. Tkachenko, N. C. Seeman, D. J. Pine, and P. M. Chaikin, "Simple quantitative model for the reversible association of DNA coated colloids," Phys. Rev. Lett., **102**, 048301 (2009)

[28]R. Dreyfus, M. E. Leunissen, R. Sha, A. V. Tkachenko, N. C. Seeman, D. J. Pine, and P. M. Chaikin, "Aggregation-disaggregation transition of DNA-coated colloids: Experiments and theory ," Phys. Rev. E, **81**, 041404 (2019)

[29]M. E. Leunissen, R. Dreyfus, R. Sha, N. C. Seeman, and P. M. Chaikin, "Quantitative study of the association thermodynamics and kinetics of DNA-coated particles for different functionalization schemes," J. Am. Chem. Soc., **132**, 1903–1913 (2010)

[30]Y. Sun, N. Harris, and C. Kiang, "Phase transition and optical properties of DNA-gold nanoparticle assemblies," Plasmonics, **2**, 193–199 (2007)

[31]A. V. Tkachenko, "Morphological diversity of DNA-colloidal self-assembly," Phys. Rev. Lett., **89**, 148303 (2002)

[32]T. Chen, M. Lamm, and S. Glotzer, "Biomolecule-directed assembly of nanoscale building blocks studied via lattice Monte Carlo simulation," J. Chem. Phys., **121**, 3919–3929 (2004)

[33]D. B. Lukatsky and D. Frenkel, "Phase behavior and selectivity of DNA-linked nanoparticle assemblies," Phys. Rev. Lett., **92**, 068302 (2004)

[34]D. B. Lukatsky and D. Frenkel, "Surface and bulk dissolution properties, and selectivity of DNA-linked nanoparticle assemblies," J. Chem. Phys., **122**, 214904 (2005)

[35]H. Xiong, D. van der Lelie, and O. Gang, "Phase behavior of nanoparticles assembled by DNA linkers," Phys. Rev. Lett., **102**, 015504 (2009)

[36]B. Bozorgui and D. Frenkel, "Liquid-vapor transition driven by bond disorder," Phys. Rev. Lett., **101**, 045701 (2008)

[37]A. J. Kim, R. Scarlett, P. L. Biancaniello, T. Sinno, and J. C. Crocker, "Probing interfacial equilibration in microsphere crystals formed by DNA-directed assembly," Nature Materials, **8**, 52–55 (2009)

[38]R. T. Scarlett, J. C. Crocker, and T. Sinno, "Computational analysis of binary segregation during colloidal crystallization with DNA-mediated interactions," J. Chem. Phys., **132**, 234705 (2010)

[39]W. Dai, S. Kumar, and F. Starr, "Universal two-step crystallization of DNA-functionalized nanoparticles," Soft Matter, doi 10.1039/b000000x (2010)

[40]F. Martinez-Veracoechea, B. Bozorgui, and D. Frenkel, "Anomalous phase behavior of liquid-vapor phase transition in binary mixtures of DNA-coated particles," Soft Matter, doi 10.1039/c0sm00567c (2010)

[41]M. Mammen, S. Choi, and G. M. Whitesides, "Polyvalent interactions in biological systems: Implications for design and use of multivalent ligands and inhibitors," Angew. Chem. Int. Ed., **37**, 2754–2794 (1998)

[42]L. Kiessling, J. Gestwicki, and L. Strong, "Synthetic multivalent ligands in the exploration of cell-surface interactions," Curr. Opin. Chem. Biol., **4**, 696–703 (2000)

[43]W. H. Taylor and P. J. Hagerman, "Application of the method of phage T4 DNA ligase-catalyzed ring-closure to the study of DNA structure. II. NaCl-dependence of DNA flexibility and helical repeat." J. Mol. Biol., **212**, 363–376 (1990)

[44]W. Press, S. Teukolsky, W. Vetterling, and B. Flannery, *Numerical Recipes in FORTRAN* (Cambridge Univ. Press, Cambridge, 2001)

[45]A. Zilman, J. Kieffer, F. Molino, G. Porte, and S. Safran, "Entropic phase separation in polymer-microemulsion networks," Phys. Rev. Lett., **91**, 015901 (2003)

[46]P. I. Kitov and D. R. Bundle, "On the nature of the multivalency effect: a thermodynamic model," J. Am. Chem. Soc., **125**, 16271–16284 (2003)

[47]S. J. Hurst, H. D. Hill, and C. A. Mirkin, ""Three-dimensional hybridization with polyvalent DNA-gold nanoparticle conjugates," J. Am. Chem. Soc., **130**, 12192–12200 (2008)

[48]H. D. Hill, S. J. Hurst, and C. A. Mirkin, "Curvature-induced base pair "slipping effects in DNA-nanoparticle hybridization," Nano Lett., **9**, 317–321 (2009)

[49]J. J. SantaLucia, "A unified view of polymer, dumbbell, and oligonucleotide DNA nearest-neighbor thermodynamics," Proc. Natl. Acad. Sci. USA, **95**, 1460–1465 (1998)

[50]R. Hunter, *Foundations of Colloid Science* (Oxford Univ. Press, Oxford, 1992)

[51]J. Gibbs-Davis, G. Schatz, and S. Nguyen, "Sharp melting transitions in DNA hybrids without aggregate dissolution: proof of neighboring-duplex cooperativity," J. Am. Chem. Soc., **129**, 15535–15540 (2007)

[52]G. Vliegenthart and H. Lekkerkerker, "Predicting the gas-liquid critical point from the second virial coefficient," J. Chem. Phys., **112**, 5364–5369 (2000)

[53]M. Noro and D. Frenkel, "Extended corresponding-states behavior for particles with variable range attractions," J. Chem. Phys., **113**, 2941–2944 (2000)

[54]V. Anderson and H. Lekkerkerker, "Insights into phase transition kinetics from colloid science," Nature, **416**, 811–815 (2002)

[55]R. J. Macfarlane, B. Lee, H. D. Hill, A. J. Senesi, S. Seifert, and C. A. Mirkin, "Assembly and organization processes in DNA-directed colloidal crystallization," Proc. Nat. Acad. Sci. USA, **106**, 10493–10498 (2009)

[56]T. Drummond, M. G. Hill, and J. Barton, "Electrochemical DNA sensors," Nature Biotechnology, **21**, 1192–1199 (2003)

[57]T. A. Taton, C. Mirkin, and R. Letsinger, "Scanometric DNA array detection with nanoparticle probes," Science, **289**, 1757–1760 (2000)

[58]J. Reichert, A. Csaki, J. Kohler, and W. Fritzsche, "Chip-based optical detection of DNA hybridization by means of nanobead labeling," Anal. Chem., **72**, 6025–6029 (2000)